AD-A131 634 IMPROVED WAVE DRAG PREDICTIONS USING MODIFIED LINEAR THEORY(U) VOUGHT CORP DALLAS TX R T STANCIL 07 DEC 82 2-55110/2R-53299 DTNSRDC-ASED-CR-1-83 N00167-82-C-0023 1/1

UNCLASSIFIED F/G 20/4 NL

END

DATE FILMED

9 - 83

DTIC

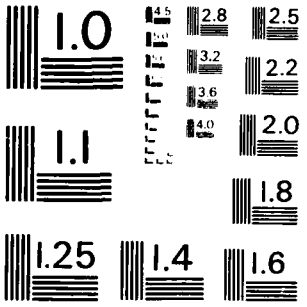

VOUGHT R AND D

DTNSRDC-ASED-CR-1-83

IMPROVED WAVE DRAG PREDICTIONS USING MODIFIED LINEAR THEORY

R. T. STANCIL

VOUGHT CORPORATION
an LTV company

Post Office Box 225907 Dallas, Texas 75265

7 December 1982

Final Technical Report

APPROVED FOR PUBLIC RELEASE: DISTRIBUTION UNLIMITED

PREPARED UNDER CONTRACT NO. N00167-82-C-0023 FOR

DAVID TAYLOR NAVAL SHIP R&D CENTER
BETHESDA, MD.

AND

NASA/LANGLEY RESEARCH CENTER
HAMPTON, VA.

UNCLASSIFIED

SECURITY CLASSIFICATION OF THIS PAGE (When Data Entered)

REPORT DOCUMENTATION PAGE		READ INSTRUCTIONS BEFORE COMPLETING FORM
1. REPORT NUMBER DTNSRDC-ASED-CR-1-83	2. GOVT ACCESSION NO. A131634	3. RECIPIENT'S CATALOG NUMBER
4. TITLE (and Subtitle) IMPROVED WAVE DRAG PREDICTIONS USING MODIFIED LINEAR THEORY		5. TYPE OF REPORT & PERIOD COVERED Final Technical Report 7 Dec. 1981 - 7 Dec. 1982 6. PERFORMING ORG. REPORT NUMBER 2-55110/2R-53299
7. AUTHOR(s) R. T. Stancil		8. CONTRACT OR GRANT NUMBER(s) N00167-82-C-0023
9. PERFORMING ORGANIZATION NAME AND ADDRESS Vought Corporation P. O. Box 225907 Dallas, Texas 75265		10. PROGRAM ELEMENT, PROJECT, TASK AREA & WORK UNIT NUMBERS
11. CONTROLLING OFFICE NAME AND ADDRESS David Taylor Naval Ship R&D Center Code 5322:LSB Bethesda, MD 20084		12. REPORT DATE 7 Dec. 1982 13. NUMBER OF PAGES 82
14. MONITORING AGENCY NAME & ADDRESS (if different from Controlling Office)		15. SECURITY CLASS. (of this report) Unclassified 15a. DECLASSIFICATION DOWNGRADING SCHEDULE N/A

16. DISTRIBUTION STATEMENT (of this Report)

APPROVED FOR PUBLIC RELEASE: DISTRIBUTION UNLIMITED

17. DISTRIBUTION STATEMENT (of the abstract entered in Block 20, if different from Report)

18. SUPPLEMENTARY NOTES

19. KEY WORDS (Continue on reverse side if necessary and identify by block number)

Supersonic drag, wave drag, modified linear theory

20. ABSTRACT (Continue on reverse side if necessary and identify by block number)

The wave drag prediction method is based on a modified supersonic linear theory computer technique developed in this contract and two earlier contracts, N00167-78-C-0005 and N00167-79-C-0123, all of which were jointly funded by DTNSRDC and NASA/Langley Research Center. The modified linear theory differs from ordinary linear theory in that it uses the exact boundary condition, it uses the local perturbed velocity to calculate $\beta = \sqrt{M^2 - 1}$, it uses the exact pressure coefficient equation, and it uses characteristic tracing to determine

DD FORM 1 JAN 73 1473 EDITION OF 1 NOV 65 IS OBSOLETE

S/N 0102-LF-014-6601

UNCLASSIFIED

SECURITY CLASSIFICATION OF THIS PAGE (When Data Entered)

20. regions of influence. The theoretical and numerical techniques are described in detail. A computer user's manual is included which provides a detailed description of the inputs and outputs of the computer routine, including recommended guidelines for preparing the geometric input. Comparisons between predictions of drag or pressures using the modified linear theory are made for five cases with wind tunnel data or other theories. These comparisons verify the improved accuracy of the modified linear theory relative to ordinary linear theory, particularly for high Mach numbers and high surface slopes.

TABLE OF CONTENTS

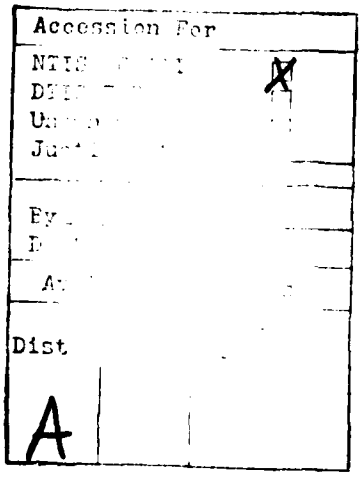

LIST OF FIGURES

ABSTRACT

This document provides the final report for Contract Number N00167-82-C-0023, "Applications of an Improved Wave Drag Prediction Method." The method is based on a modified supersonic linear theory computer technique developed in this contract and two earlier contracts, N00167-78-C-0005 and N00167-79-C-0123, all of which were jointly funded by DTNSRDC and NASA/Langley Research Center. The modified linear theory differs from ordinary linear theory in that it uses the exact boundary condition, it uses the local perturbed velocity to calculate $\beta = \sqrt{M^2-1}$, it uses the exact pressure coeffficient equation, and it uses characteristic tracing to determine regions of influence. The theoretical and numerical techniques are described in detail. A computer user's manual is included which provides a detailed description of the inputs and outputs of the computer routine, including recommended guidelines for preparing the geometric input. Comparisons between predictions of drag or pressures using the modified linear theory are made for five cases with wind tunnel data or other theories. These comparisons verify the improved accuracy of the modified linear theory relative to ordinary linear theory, particularly for high Mach numbers and high surface slopes.

IMPROVED WAVE DRAG PREDICTIONS USING MODIFIED LINEAR THEORY

1.0 INTRODUCTION

Supersonic linearized theory, including the special cases of slender body theory and area rule, have well known limitations. While linear theory does remarkably well in predicting lift and pitching moment, it does not do as well in predicting drag. The largest discrepancies occur when the sweep angle is nearly equal to the Mach angle ($\cos^{-1}1/M$). Inaccurate prediction results because drag is the integral of pressure times local slope, and the largest errors in predicted pressure are likely to occur where the slopes are largest. Van Dyke's second-order method gives much improved accuracy relative to slender-body or linear theory results for two-dimensional flow, either planar or axisymmetric, but a method for extending it to three dimensions has not been found. For aircraft configurations, analytical methods for predicting drag more accurately than area rule have not been found, short of the very complex "exact" solutions such as method of characteristics, time-dependent equations of motion, or relaxation techniques. These exact methods require large amounts of computer time and are often sensitive to input data smoothness, choice of arbitrary parameters, etc. These techniques are not ideal for preliminary design, where many answers are required quickly. Preliminary design requires a method which approximates linear theory in complexity and approaches the exact solutions in accuracy. The modified linear theory technique has been developed to provide an efficient, accurate method.

The analytical and numerical techniques used in the modified linear theory analysis routine are described. Calculations for several cases are compared with wind tunnel data or other theoretical methods. A computer user's manual is included as Appendix B.

2.0 LINEAR THEORY PERTURBATION RELATIONS

Because line distributions of sources and sinks are inadequate for a general three-dimensional solution, all calculations described in this paper utilize surface distributions of sources and sinks. The velocity potential equation is

$$\phi(x,y,z) = \frac{-V_0}{\pi} \iint \frac{S(x_1,y_1,z_1)\,dx_1\,dy_1}{\sqrt{(x-x_1)^2-\beta^2[(y-y_1)^2+(z-z_1)^2]}}$$

where S is the souce strength, ds = $\sqrt{dx_1^2+dz_1^2}$ on the surface of the body, and the integral is taken over that portion of the surface included in the Mach forecone from the point x,y,z. Now, under certain nonrestrictive conditions, the perturbation velocity components can be derived to be of the form

$$u = \phi_x = \frac{-V_0 S(x,y,z)}{\sqrt{x^2-\beta^2(y^2+z^2)}} + \frac{1}{\pi}\iint \frac{G}{r}\,dx_1\,dy_1$$

$$v = \phi_y = \frac{-V_0 y}{\sqrt{x^2-\beta^2(y^2+z^2)}} + \frac{1}{\pi}\iint \frac{H}{r}\,dx_1\,dy_1$$

$$w = \phi_z = \frac{-V_0 z}{\sqrt{x^2-\beta^2(y^2+z^2)}} + \frac{1}{\pi}\iint \frac{I}{r}\,dx_1\,dy_1$$

where ε is the local slope, v_n is the perturbation component perpendicular to the freestream and normal to v_p, and v_p is the perturbation component perpendicular to the freestream and parallel to the local surface. The functions F, G, and H are dependent on the value of β, the limits of integration, the geometry of the model, and the functions used to describe the variations of source strength in the y, z directions.

3.0 MODIFICATIONS TO LINEAR THEORY

The accuracy of the current method results from the combined effects of the exact boundary condition, and use of the local (perturbed) value of $\beta = \sqrt{M^2 - 1}$. The exact pressure coefficient equation is also used.

The exact boundary condition (Fig. 1) requires not only the use of the perturbed streamwise velocity component but also the determination of the surface slope (ε) in the plane defined by the freestream velocity vector and the normal to local surface. This three-dimensional determination of the slope and the velocity component boundary conditions is necessary even in quasiplanar cases, such as for wings.

The primary effect of the local β (Fig. 2) is on the constant of proportionality, $1/\beta$. The $1/\beta$ factor appears in every term but one on the right side of Eqs. (2-4). Thus, it has a direct effect on each of the perturbation velocities. As the local Mach number approaches 1.0, the value of $1/\beta$ approaches infinity. This is obviously an undesirable result. Therefore, a correlated local Mach or β has been developed based on calculations for two-dimensional ramps and cones. The correlation puts a limit on the maximum value of $1/\beta$ and causes the correlated value to approach the limit more slowly than with the exact equation. The effect of local β on the region of influence (characteristic directions) is less pronounced, particularly for two-dimensional cases, either planar or axisymmetric. However, for three-dimensional flow the variations in propagation direction can be important because of the lateral or longitudinal displacement of interference effects. Region of influence effects will be discussed further below.

The two modifications have opposite effects. For compressions, the exact tangency condition tends to reduce the magnitude of the perturbations because $(1 + \phi_x/V_o)$ is less than unity, and the required normal velocity v_n is less than with the linearized boundary condition. But the local β in Eqs. (2-4) tends to increase the perturbations values because, when M is smaller than the freestream value, $1/\beta$ is larger. Conversely, for expansions, $(1+\phi_x/V_0) > 1$, and the required v_n is larger than the linearized values, but $1/\beta$ is smaller than the freestream value.

Theoretical pressures predicted by the modified method are compared with exact theory and linearized theory for 45-deg swept ramps (Fig. 3). The modified linear theory shows greatly improved correlation with exact theory relative to ordinary linear theory for both expansions and compressions. Also, where the lineary theory predicts infinite perturbations at sonic edge conditions for the swept ramp in Fig. 3 ($M_0 = \sqrt{2}$), the modified theory on the expansion side shows no tendency toward infinity. Use of the local β eliminates expansion singularities because $1/\beta$ approaches zero with finite positive perturbations. On the compression side, the exact and modified theories cannot be computed at $M_0 = \sqrt{2}$ for this two-dimensional case

because the flow could not actually remain two-dimensional. However, it can be seen that the modified theory will not predict infinite perturbations here either, because as $\phi_x / V_o \longrightarrow -1$, exact boundary conditions cause v_n and the source strength to approach zero. Thus, an equilibrium must be reached with the value of ϕ_x / V_o between 0 and -1.0.

4.0 ANALYTICAL AND NUMERICAL TECHNIQUES

An important numerical technique which allows the efficient evaluation of the perturbation velocity integrals in Eqs. (2) - (4) is the use of Simpson's Rule combined with stepping off from every integration limit by 0.07 times the step size. For example, the exact value of the integral

$$I = \int_0^2 \frac{dx}{\sqrt{x(2-x)}} \qquad (5)$$

is $\pi = 3.1416$. Even though there is a square root singularity at both limits, a two step (minimum) Simpson's Rule integration with the 0.07 offset gives

$$I = \frac{1}{3}\left[\frac{1}{\sqrt{.07(1.93)}} - \frac{4}{1} + \frac{1}{\sqrt{1.93(.07)}}\right] = 3.$$

which is accurate to 0.2%. The 0.07 offset is used at all times. Thus, no special treatment is required for singularities, and the offset is small enough that its effect on non-singular integrands is negligible. This technique was derived by the author for the square root and logarithmic singularities which frequently occur in linearized aerodynamic theory.

A brief discussion of the reasons for choosing the format of Eqs. (1) - (4) is in order. First, source distributions are used rather than higher order singularities because they are simpler, and because they are adequate to describe the flow around bodies with thickness except possibly at thin trailing, side or subsonic leading edges where the upper and lower surface pressures are not equal. The assumed source strengths vary linearly in both directions on a panel and are continuous across panel boundaries unless the slope is discontinuous. This continuity of source strengths and the fact that the panels can be curved in both directions allows the use of larger (i.e., fewer) panels to describe a configuration than would otherwise be possible.

Second, the form of Eqs. (2) - (4) was chosen for the following reasons. The velocity components must be obtained from derivatives of the potential function. The double integral in the potential equation cannot readily be evaluated analytically and at least one integration must be performed numerically. Numerically evaluated derivatives are highly unreliable, particularly for the derivative of a numerically evaluated integral. A much more reliable, accurate and efficient method is to perform one integration analytically, differentiate analytically for the three velocity components, and then perform the remaining integration numerically for each velocity

component. Having selected this method, the question remains of which integration to perform analytically, the streamwise or lateral? Both options were examined. It was found that analytically integrating laterally gave a simpler integrand with fewer singularities and was much more compatible with the translations required for characteristic tracing. The derivations of Eqs. (2) - (4) for laterally curved and flat panels are in Appendix A.

Because the perturbation velocities are strong functions of the local $\beta = \sqrt{M^2 - 1}$, and the local β is a function of the perturbed velocity, an iteration is required. For the first pass, a rough estimate of the perturbation velocities and β is made, based on the local slopes. This provides faster convergence than using freestream β as the first guess. A marching solution scheme is used. The iteration is performed at the front of the configuration, then at the mid-points of the first row and then at the aft end of the first row. At the front of succeeding rows, values of source strength and β from the aft end of the first row are used with interpolation as needed if the slopes are continuous. If slopes are not continuous across the row, two-dimensional or conical solutions are iterated upon. Then the solution is stepped back to the mid-points of each row, etc. This process makes the iterations more stable, as points on the back rows are not perturbed by variations in local β and source strength on preceding rows.

Variations in panelling techniques were investigated and two significant effects were found: lateral curvature and continuity between panels. The panel edges must be defined identically from one panel to the next to avoid differences in and/or negative square roots in the hyperbolic radius

$$\sqrt{\left(\frac{x - x_1}{\beta}\right)^2 - (y - y_1)^2 - (z - z_1)^2}$$

calculations. Differences in the hyperbolic radius values, particularly if near the singularity or zero value, can cause large errors in the integrand because the net effect of all the panels is a small differences of large numbers. The following conclusions regarding curvature effects are based on the format of Eqs. (2) - (4) and might be different if, for example, the streamwise integration were performed analytically. Longitudinal curvature is not important; i.e., if the exact value of slope is used in the boundary condition and no gaps are artificially introduced, the exact ordinate or streamwise curvature has a negligible effect. Lateral curvature is important, however. In the vicinity of the receiving point and along the characteristics, it is necessary to use the curved panel solution from Appendix A. Each panel is approximated by a circular arc segment. The curvature effect is used for at least two full panel widths away from each characteristic. However, when $x_1 \leq X^*$, the flat panel analysis is entirely adequate. X^* is defined as the streamwise location where the complete circle corresponding to the circular arc approximation to a given panel lies entirely within the forecone from the receiving point.

The curvature effect is used only for the laterally constant source strength. The curved panel solution with lateral source strength variation, besides being quite complex, gave undesirably large contributions in some cases. The flat panel solution for lateral source strength variation appears to be more accurate and reliable, and so it is used even on curved panels.

Two values of β are used in the method. The true local β is used to trace the characteristics, or region of influence boundaries. The true local Mach and β are computed from the exact isentropic relation:

$$M_r = \frac{M_\infty (V/V_\infty)}{\sqrt{1 + 0.2 M_\infty^2 [1 - (V/V_\infty)^2]}}$$

$$\beta_r = \sqrt{M_r^2 - 1}$$

The correlated β is used in the perturbation velocity equations. The correlated β is determined by solving for the value which would make the modified linear theory agree with a two-dimensional Prandtl-Meyer corner solution with the same (V/V_0). From the modified linear theory for a two-dimensional corner,

$$\phi_x = -\frac{V_0 S}{\beta(1-\beta\epsilon)}$$

$$\phi_z = \frac{V_0 S}{1-\beta\epsilon} \tag{8}$$

or

$$\phi_z = -\beta\phi_x \tag{9}$$

Now the Prandtl-Meyer angle is

$$\nu = \sqrt{\frac{\gamma+1}{\gamma-1}}\tan^{-1}\sqrt{\frac{\gamma-1}{\gamma+1}(M_T^2-1)} - \tan^{-1}\sqrt{M_T^2-1} \tag{10}$$

and for $\gamma = 1.4$,

$$\sqrt{\frac{\gamma+1}{\gamma-1}} = 2.2495$$

or

$$\nu = 2.2495\tan^{-1}\left(\frac{1}{2.2495}\sqrt{M_T^2-1}\right) - \tan^{-1}\sqrt{M_T^2-1}$$

The exact Prandtl-Meyer corner solution is:

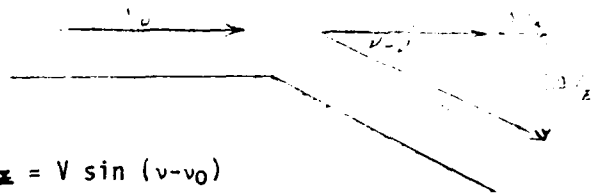

$$-\Delta V_Z = -\phi_z = V\sin(\nu-\nu_0)$$

$$\Delta V_X = \phi_x = V\cos(\nu-\nu_0) - V_0 \tag{13}$$

Substituting Eq. (13) into (9), we get

$$V\sin(\nu-\nu_0 = \beta[V\cos(\nu-\nu_0) - V_0]$$

or

$$\beta_{corr.} = \frac{\sin(\nu-\nu_0)}{\cos(\nu-\nu_0) - V_0/V}$$

where both the numerator and denominator are positive for expansions ($V > V_0$) and both are negative for compressions ($V < V_0$). The Prandtl-Meyer solution is exact for expansions, and it is also the exact isentropic solution for

compressions. The difference between pressure coefficients on two-dimensional ramps with and without shock effects are less than 2% for values of $C_p \leq 0.5$ and $M_0 < 2.6$ as shown in Figure 4. Eq. (15) is used to evaluate the correlated β except when $\beta_{corr.} > 10$ it is set to 10, and when true local Mach number is less than 1.4, a smooth transition is made from Eq. (15) at $M_T = 1.4$ to $\beta_{corr} = 0.5$ at $M_T \leq 1.0$.

Evaluation of test cases on swept ramps indicate that much better accuracy is obtained when the characteristics are not yawed even though there is a lateral velocity component. But the lateral velocity component should be included in evaluating V/V_0 for the β calculations.

It is not clear whether the β used in the integrands should be the value at the receiving point, at the sending points, or some average. In most cases, the difference was found to be negligible so the receiving point value was used. But finally, a case was found where the choice of β made a difference. On a cockpit-like forebody, where the slopes were approaching zero after being negative, the method predicted pressure much too high. This was corrected by using an averaged β in the integrands defined by

$$\beta_{avg} = \frac{1}{2}\beta_S + \frac{1}{2}\frac{\beta_L + \beta_R}{2}$$

where X_R is the X of the receiving point, X_S is the X of the sending point, and β_L and β_R are the local correlated β's on the left-running and right-running characteristics, respectively. Use of the averaged β eliminated the overprediction of pressure behind the canopy and had no effect elsewhere.

The relative advantages of characteristic tracing versus the usual linear theory see-through integration boundaries will be examined. A typical plot of the integrand in Eq. (2) for an axisymmetric body is shown in Fig. 5. The singularity at X^* is first order (i.e., of the form $1/x$) and thus produces an infinite result for integration from one side to the singularity, but the integrand is equal and opposite at $x_1 = x^* + \delta$ and $x_1 = x^* - \delta$. Therefore, the result of the total integration is finite if the source strength is continuous. But, if the body has a slope discontinuity, the source strength is discontinuous, and at a point located behind the corner such that x^* is equal to the x of the corner, the perturbation velocities are theoretically infinite. It is obviously incorrect to get an infinite perturbation from an area which actually cannot influence the point under consideration. If characteristic tracing is performed, the point at $x_1 = x^*$ and $\mu = \tau$ will be outside of the influencing region. With the integration taken only to the characteristic line, the integrand is finite everywhere.

The equations for the rate of lateral translation of the characteristics or the forecone are presented. Let y_i' be the local surface lateral direction at the characteristic, and z_i' the local surface outward normal direction. For unyawed characteristic tracing, we get the simple result:

$$\frac{dy_i'}{dx_i} = \pm \frac{\sqrt{1 + \varepsilon^2}}{\beta}$$

For the see-through case, the rate is:

$$\frac{dy_1'}{dx_1} = \frac{\frac{X-X_1}{\beta^2} - \varepsilon z'}{y} \qquad \text{for } X > X_1$$

$$\frac{dy_1'}{dx_1} = \pm \frac{\sqrt{1 - \beta^2\varepsilon^2}}{\beta} \qquad \text{for } X = X_1$$

where y' and Z' are the coordinates of the receiving point relative to the sending panel. The see-through rate is derived from:

$$\sqrt{\left(\frac{x-x_1}{\beta}\right)^2 - (y-y_1)^2 - (z-z_1)^2} = 0 \quad \text{and} \quad \frac{dz}{dx} = \varepsilon \quad \text{at} \quad x' = 0, \; z' = 0$$

The usual linear theory (or see-through) integration boundaries are compared with the actual characteristic boundaries in Figure 6. For point A, the difference in the influencing region is not great. At point B, the see-through method is obviously unusable with surface sources because the Mach forecone does not include the surface anywhere near point B. This condition occurs when $\beta\varepsilon \leq -1$, and while extreme, it does occur on a fineness ratio 4 circular arc body at Mach numbers of 2.0 and above. The method is also usable when $\beta\varepsilon \geq +1$.

As shown in Reference 1, the characteristic tracing method is more accurate for moderate-to-high-angle cones, while the see-through method is better at predicting the maximum expansion pressures on slender circular arc bodies.

The characteristic tracing technique eliminates contributions from areas which cannot influence the receiving point, such as a strut or pod on the lower side of a wing which cannot affect the upper surface of the wing. However, for multi-bodies and bodies with step discontinuities such as inlets, the characteristic tracing adds considerable complexity to the computer logic required. The complexity arises because of multiple possibilities for determining regions of influence. When a receiving point is downstream of a step, the region of influence of panels upstream of the step can be determined by: (a) the tracing through space of a characteristic from anywhere along the step, (b) the tracing of a characteristic from the edge of the step along the surface, or (c) the tracing of a characteristic along the surface from any location defined by (a) above. In addition, these complex regions of influence can be different for different receiving points, so the calculation can not be done once and used repeatedly.

It is concluded that the characteristic tracing method is superior to the see-through because of; 1) the elimination of the infinite perturbation from a slope discontinuity; 2) the capability to calculate accurately when $\beta\varepsilon \leq -1$ and to calculate with $\beta\varepsilon > 1$; 3) better numerical accuracy on moderate-and high-angle cones; and 4) the elimination of contributions from areas which cannot actually influence the point being considered. These benefits outweigh the overprediction of maximum expansion pressures on slender circular arc bodies and the additional complexity of the calculations.

Having selected the characteristic tracing method, translation of the receiving point coordinates is required to maintain proper values of the hyperbolic radius. For axisymmetric bodies, the only translation required is an x translation. For correct results, it was found necessary to keep the hyperbolic radius value equal to zero on the characteristics in the vicinity

of the receiving point. By numerical experimentation, this "vicinity" was defined by the angular difference between the y - z projection of the surface normal at the receiving point and the normal on the characteristic being less than cos (0.16) = 80.8°. After a characteristic has left the "vicinity" of the receiving point, the x margin from the forecone (hyperbolic radius = 0) to the characteristic is allowed to become positive but it is not allowed to decrease. I.e., As the characteristics are traced forward, x translation will be done if necessary so that the margin is always greater than or equal to the margin at the previous point on the same characteristic. The translated receiving point coordinates (Qx, Qy, Qz) are single-valued functions of x_1, the x integration variable.

For non-axisymmetric bodies, y and z translation may be required. The y, z shifting will be considered in two parts. The lateral part is in the direction parallel to a line between the two characteristics, and the vertical part is perpendicular to the same line.

The lateral translation is required on general body shapes so that the hyperbolic radius can be zero on both characteristics in the vicinity of the receiving point, and to maintain the proper margins or values when one or both characteristics are not in the vicinity.

Vertical translation is required to prevent bulges such as canopies from projecting into or near to the forecone from a point behind the canopy. This is not a problem caused by characteristic tracing; rather, it can be handled because of characteristic tracing. At a given x_1, all panel edges between the characteristics are tested and Qy and Qz are shifted according to the most critical panel edge and the criteria $z_{c_2} \geq r_1/3$,

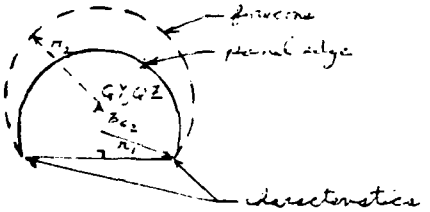

where r_1 is the radius of the circle passing through the panel edge and the two characteristics, and r_2 is the radius of the forecone at X_1.

On some general body shapes, the use of characteristic tracing results in an anomaly. This anomaly cannot occur on axisymmetric bodies, but will occur on shapes such as elliptic cones or bodies with flat or concave surfaces, for example. When the inward normal from a characteristic trace has passed through the y-z projection of the receiving point, the value of hyperbolic radius increases as the characteristic is approached laterally instead of decreasing or approaching zero. Usually, on a panel cut by a characteristic, the integrand has the opposite sign relative to neighboring panels. But when the hyperbolic radius increases to the characteristic, the integrand has the same sign as neighboring panels and larger magnitude, resulting in a large, erroneus contribution from panels which are on the opposite side of the body from the receiving point. This large undesirable contribution has been eliminated by neglecting the integrand when the above-mentioned condition exists and a lateral limit is a characteristic.

The non-integral terms in Eqs. (A-21), (A-22), (A-29) and (A-30) occur at the receiving point when the point is on the body, and they also occur in most cases when the forecone intersects a nearby body or when two panels intersect laterally at approximately a right angle.

Consider a single panel with a side edge at y_S.

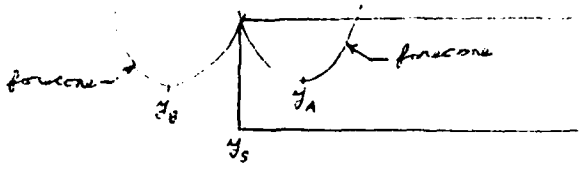

When $y>y_A$, the non-integral term is a unit value and is the entire effect, because the integrands are zero. When $y>y_S$, the non-integral term is also the unit value, but at $y=y_S$ it is half of the unit value, and when $y<y_S$, it is zero. The integral contribution is such that the net effect varies smoothly from the unit value at $y=y_A$ through one-half at $y=y_S$ to zero at $y=y_B$.

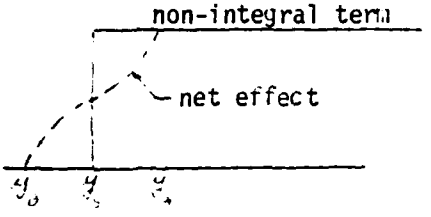

It was found that the numerical integrals in Eqs. (A-29) and (A-30) could be significantly in error at a lateral corner because the term $(X-X_1)^2/\beta^2 - (Z-Z_1)^2$ in the denominator becomes very small. In the vicinity of the characteristic, let $X_1 = X_S - t$, where $(X-X_S)^2/\beta^2-(Z-Z_S)^2 - (y-y_S)^2 = 0$. Then the singular and near-singular terms are of the form:

$$I = \int_0 \frac{dt}{\left[\left(\frac{X-X_S+t}{\beta}\right)^2-(Z-Z_S+\epsilon t)^2\right]\sqrt{\left(\frac{X-X_S+t}{\beta}\right)^2-(Z-Z_S+\epsilon t)^2-(y-y_S)^2}} \qquad (20)$$

$$= \int_0 \frac{dt}{\left[(y-y_S)^2+2\left\{\frac{X-X_S}{\beta^2}-\epsilon(Z-Z_S)\right\}t+\left(\frac{1}{\beta^2}-\epsilon^2\right)t^2\right]\sqrt{2\left\{\frac{X-X_S}{\beta^2}-\epsilon(Z-Z_S)\right\}t+\left(\frac{1}{\beta^2}-\epsilon^2\right)t^2}}$$

If we neglect the second order terms in t, we have:

$$I = K\int_0^T \frac{dS}{(Y_1^2+2S)\sqrt{S}} \qquad (21)$$

where

$$S = \left\{\frac{X-X_S}{\beta^2}-\epsilon(Z-Z_S)\right\}t$$

$$Y_1 = y-y_S$$

$$T = \Delta X_1\left\{\frac{X-X_S}{\beta^2}-\epsilon(Z-Z_S)\right\}$$

Analytically

$$\int_0^T \frac{dS}{(Y_1^2+2S)\sqrt{S}} = \sqrt{\frac{2}{Y_1^2}}\tan^{-1}\sqrt{\frac{2T}{Y_1^2}} \qquad (22)$$

If we apply a ratio to the Simpson's Rule contribution at the usual .07 offset, and set the Simpson's Rule result equal to the analytical result, we can solve for the required ratio. Note $\Delta X_{\text{above}} = 2\Delta X_{\text{Simpson's}}$.

$$\frac{T/2}{3}\left[\frac{1}{(2T+Y1^2)\sqrt{T}} + \frac{4}{(T+Y1^2)\sqrt{T/2}} + \frac{RATIO}{(.07T+Y1^2)\sqrt{.035T}}\right] = \sqrt{\frac{2}{Y1^2}}\tan^{-1}\sqrt{\frac{2T}{Y1^2}} \qquad (23)$$

$$RATIO = \sqrt{.035}\left(1+.07T/Y1^2\right)\left[\frac{12}{\sqrt{2T/Y1^2}}\tan^{-1}\sqrt{\frac{2T}{Y1^2}} - \frac{1}{1+2T/Y1^2} - \frac{4\sqrt{2}}{1+T/Y1^2}\right] \qquad (24)$$

This ratio is applied at the endpoint of the integrals in Eqs. (A-21) and (A-22) or (A-29) and (A-30) when $(Z-Z_S) > |y-y_S|$, there is a lateral discontinuity at the panel edge defining the lateral limit of integration opposite the characteristic, and Y1 is not zero. When Y1 is zero, it can be shown that the correct limiting value will be obtained by using half of the usual non-integral term and that no ratio is needed on the integral term.

The wing solution included in the current version of the routine involves some approximations. The calculations on the wing utilize a routine which was developed earlier for wing-alone calculations. It uses a planar source sheet to represent the wing, and the boundary conditions are satisfied in the chord plane rather than on the upper and lower surfaces. Therefore, the wing solution is symmetrical; i.e., it is the same on the upper and lower surfaces. Only the normal and streamwise perturbation velocities are computed on the wing. The lateral velocity is assumed to vary from zero at the wing-body intersection to a maximum. The maximum occurs at the leading edge for subsonic leading edges or at and ahead of the Mach line from the wing-body intersection for supersonic leading edges. The maximum lateral component is such that the total perturbation component in the wing plane is perpendicular to the leading edge. In the wing solution, except for the effect of body on wing, a reflection plane is assumed at the wing-body intersection. Because of the planar solution, the normal velocity is equal to the source strength. The wing-on-wing solution uses the same modifications to linear theory as the body solution, except it uses see-through rather than characteristic tracing; and the free-stream (X) direction integration was done analytically. For the planar case, the analytical X integration case simplifies considerably and is more efficient computationally. The wing slopes and source strengths are fitted with cubic polynomials streamwise and parabolas spanwise.

The wing-body interferences are accounted for by first computing the wing-alone solution with a reflection plane at the wing-body intersection. Then the body solution is calculated including the effect of the wing. Finally, the streamwise perturbation velocities on the wing due to the body are determined, and the wing solution is iterated again with the body-on-wing velocities added.

For blunt noses, local subsonic flow occurs. The modified linear theory will provide a solution with local subsonic flow, but unless the local Mach number is close to 1.0, the accuracy will be poor. For this reason, a modified Newtonian solution is included in the method. The modified Newtonian solution includes an adjustment factor from Ref. 2 which provides improved accuracy at low supersonic freestream Mach numbers on hemispherical noses.

The pressure coefficient equation is:

$$C_p = C_{p_n}\left(1 - \frac{M_\infty^{3.5}}{M_\infty^{3.5} - 0.3}\sin^2\delta\right)$$

where C_{pn} is the pressure coefficient behind a normal shock wave, M_∞ is the freestream Mach number, and δ is the local slope angle. The modified Newtonian pressures are used until the local Mach number reaches 1.1. Then, a total pressure loss factor is applied to match the modified linear theory pressure to the modified Newtonian value. This pressure loss factor is then attenuated exponentially downstream. The scaling constants involved in the attenuation were determined empirically based on a small amount of data, and further analysis based on a broader data base would be highly desirable. To prevent the $(1-\beta\varepsilon)$ term in the denominator of the non-integral terms in ϕ_1 and ϕ_2 from reaching zero at $\beta\varepsilon=1$, it is replaced for $\beta\varepsilon > 0.8$ with an arbitrary function with a minimum value of 0.1 at $\beta\varepsilon = 1.0$. This is necessary to provide a reasonable solution on blunt noses. At longitudinal slope discontinuities, the exact isentropic solution is easily calculated in addition to the modified linear theory solution. When the modified linear theory solution predicts a higher pressure immediately behind the corner than the two-dimensional solution, a pressure loss factor is applied in the same manner as was done at the modified Newtonian matching point above. The pressure loss factor is again attenuated exponentially downstream.

The values of source strength, pressure coefficient, velocity components and β are all assumed to vary linearly across a panel in the lateral direction. They are continuous across panel boundaries unless there is a lateral slope discontinuity. In any given row, the number of unknown values of source strength will be the number of panels plus one, plus the number of lateral slope discontinuities. Each slope discontinuity adds an unknown because at that panel edge there are two values of source strength instead of one. The number of control points at which the boundary condition of no-flow-through is satisfied must be equal to the number of unknowns. Starting at the top centerline of the body, control points are placed near the initial panel edge and also near the opposite edge of only the last panel and the panels preceding a lateral slope discontinuity. The control points are offset from the edge by a fraction (currently equal to 0.2) of the panel width to provide better averaging in the event of non-linear variations and to avoid possible singularity problems. The assumed values of source strength and β are at the panel edges. The calculated values of perturbation velocities, β and pressure coefficient are at the control points, and these are extrapolated linearly to the panel edges for interpolation purposes and to provide the β estimates for the next iteration.

A restart capability is incorporated to allow extra prints or geometry changes at minimum cost. Using the restart capability, geometry changes can be made without having to recalculate the solution ahead of the point where the geometry changes. After the calculations for each row of panels has been completed, the pertinent common data is written to a file which can be saved, providing capability to restart the calculation for one Mach number at the beginning of any row for which all preceding row computations were completed.

5.0 COMPARISONS WITH WIND TUNNEL DATA AND OTHER THEORIES

Five cases were selected for testing the predictions of the modified linear theory against wind tunnel data or other theoretical methods. The results of these comparisons could then be used to establish the validity of the modified linear theory method. Comparisons for the five cases are discussed below.

5.1 Analytic Forebody

An analytically defined forebody shape was tested in the Langley Unitary Plan wind tunnel. Pressure data were obtained at several Mach numbers, angles-of-attack, angles of yaw, and at many body locations. These pressure data are reported in Reference 3. The modified linear theory method was used to calculate pressures on this body, called Forebody 4 in Reference 3, at zero angle-of-attack and zero yaw at the four tested Mach numbers. The body shape is shown in Figure 7. Calculated pressures are compared with the measured pressures of Reference 3 in Figures 8 through 17. The agreement is quite good considering the high slopes on portions of the body. Linear theory significantly underpredicts the pressures on the upper, forward portions of the forebody at Mach 1.7, but the modified linear theory compares well. At the higher Mach numbers, linear theory is unusable because $\beta\varepsilon$ is greater than 1.0, but the modified theory continues to compare well with the data.

5.2 Drooped Nose Bodies

A series of bodies with circular cross-sections and parametrically varying amounts of nose droop have been tested in the NASA/Langley Research Center Unitary wind tunnel. The results are to be published in the near future by Barry Shrout. One of the body shapes with sixteen degrees droop is shown in Figure 18 as displayed by the graphics routine. The pressure, or wave, drag results were obtained by subtracting estimated skin friction drag from the measured forces. Pressure drags predicted by the modified linear theory for three bodies at three Mach numbers are compared with the test data in Figure 19. The agreement is quite good, and is much better than the far field (area rule) results.

5.3 Conical Wing Body

The conical wing body consists of a symmetrical wing with blunt trailing edges and a mostly conical body underneath. The maximum thickness of the wing is at or near the trailing edge. The planform is a 57° swept delta with the outer trailing edge cut off at an angle. The body is a segment of an 8° cone over more than half its length with a transition approaching a constant section near the aft end. See Figure 20. This configuration has been tested in the NASA/Langley Research Center Unitary wind tunnel and the data are reported in Reference 4. At Mach 1.6 and a Reynolds number of 2.0×10^6/ft., the $C_{D_{min}}$ is 0.0186. Subtracting estimated skin friction drag of 0.0063 leaves a measured pressure drag of 0.0123. The modified linear theory calculation yields a pressure drag of 0.0039, consisting of 0.0014 body drag and 0.0025 wing drag. A close examination of the geometry reveals that the wing leading edge is very blunt. Also, the wing is conical to the streamwise station of the wing tip. A conical flow calculation using the modified linear theory with the wing defined as part of the body and input points concentrated near the wing leading edge yields a drag prediction of 0.0082. Thus, most of

the discrepancy is explained by the inability of the wing solution to adequately represent a shape where most of the drag occurs in the first one or two percent of the chord.

5.4 Missile With Inlets

A missile model with axisymmetric inlets was tested at NASA/Langley Research Center and the data are to be published soon by Clyde Hayes. The arrangement is shown in Figure 21. The ϕ=90° tail orientation with wings off is compared at Mach 2.5 with the wind tunnel data. The measured $C_{D_{min}}$ is 0.52 from which estimated skin friction drag of 0.20, spillage drag of 0.04, and boundary layer diverter drag of 0.02 are subtracted, for a net experimental wave drag of 0.26. Due to difficulties with the computer routine, it was necessary to run the configuration in parts: the forward body, the aft body, tails and inlet lip. The modified linear theory prediction is 0.27 for the wave drag on the body, tails, and inlet lip. This is considered to be good agreement.

5.5 Area Rule Comparisons

The axisymmetric body for this case consists of a tangent ogive nose followed by an arbitrarily "coked" section. A trapezoidal wing with 45° leading edge sweep and a 65A005 airfoil is located at two positions. See Figure 22. The forward position provides positive interference drag between wing and body and the aft position results in negative, or favorable, interference. Area rule and modified linear theory drags were calculated for Mach numbers from 1.2 to 2.0. The body alone and wing alone drags are compared in Figure 23. The body alone drags agree quite closely with the modified linear theory values being slightly higher at Mach 1.8 and 2.0. The wing alone drags agree fairly well except at the sonic edge Mach condition where the area rule drags are always high. At Mach 1.8 and 2.0 (supersonic leading edge), the modified linear theory drags are slightly higher. Interference drags and total drags for the two wing positions are shown in Figure 24. The interference drag predictions are similar, except the modified linear theory does not predict the very large interference effects at Mach 1.2 as does the area rule. Intuitively, the area rule interference effects at 1.2 Mach, particularly for the aft mounted wing, seem too large. Also, on the total drag, the modified linear theory curves are smoother because of the more reasonable results for the wing and interference drags.

6.0 CONCLUSIONS

Comparisons between wave drag and pressures as predicted by the modified linear theory and as obtained from wind tunnel tests or area rule predictions were made. In the conical wing body case, agreement was poor because of the inability of the wing portion of the routine to adequately model the extremely blunt leading edge. In the other four cases, agreement is good. For the analytic forebody, good agreement was obtained with wind tunnel measured pressures over a wide Mach number range on a shape which has high local slopes, where linear theory is unusable and area rule is highly inaccurate. On the drooped nose bodies, pressure drags predicted by the modified linear theory agree well with the wind tunnel data for the three droop angles and three Mach numbers. For the missile with inlets, wave drag calculated by the modified linear theory agreed with wind tunnel data for the one case examined. In the area rule comparisons, the modified linear theory drags

agreed well with the area rule values except in a few areas where there is reason to believe that the modified linear theory results are more realistic than the area rule values. It is concluded that the accuracy of the modified linear theory has been verified.

It is recommended that the modified linear theory be used to predict supersonic pressures and wave drag on any bodies and wing-bodies which include areas of moderate to high local slopes, or which have any areas including wing leading edges which have supersonic edges ($\beta\varepsilon \geq 1$). It is also recommended that the computer routine be improved to make it more efficient, general and reliable.

REFERENCES

1. Stancil, R. T., "Improved Wave Drag Predictions Using Modified Linear Theory," AIAA Journal of Aircraft, Vol. 16, Number 1, January 1979, pp. 41-46.

2. Brickman, J.E., "The Determination of Flow Over Blunt Nose Bodies of Revolution at Transonic and Supersonic Speeds," Master's Thesis, Univ. of Tulsa, 1964.

3. Townsend, James C.; Howell, Dorothy T.; Collins, Ida K.; and Hayes, Clyde, "Surface Pressure Data on a Series of Analytic Forebodies at Mach Numbers From 1.70 to 4.50 and Combined Angles of Attack and Sideslip," NASA TM 80062, June 1979.

4. Miller, David S.; Landrum, Emma Jean; Townsend, James C.; and Mason, William H., "Pressure and Force Data for a Flat Wing and a Warped Conical Wing Having a Shockless Recompression at Mach 1.62," NASA TP-1759, April 1981.

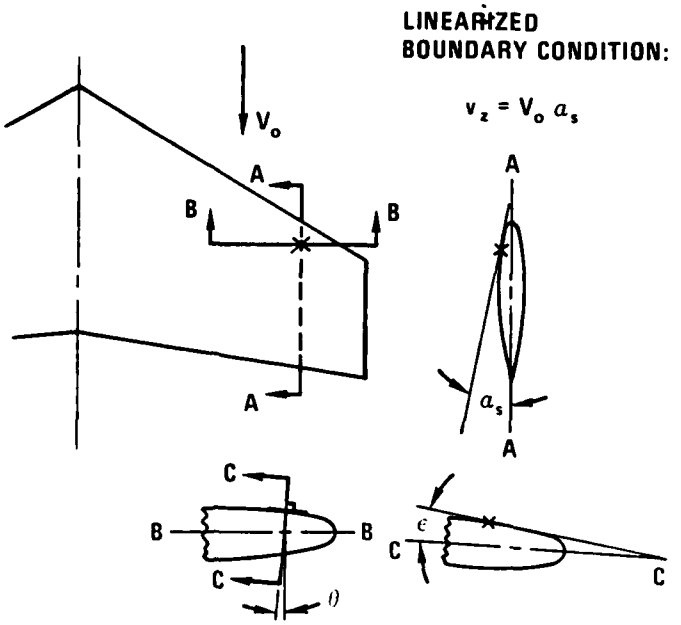

Fig. 1 Modification #1 - Exact Boundary Condition

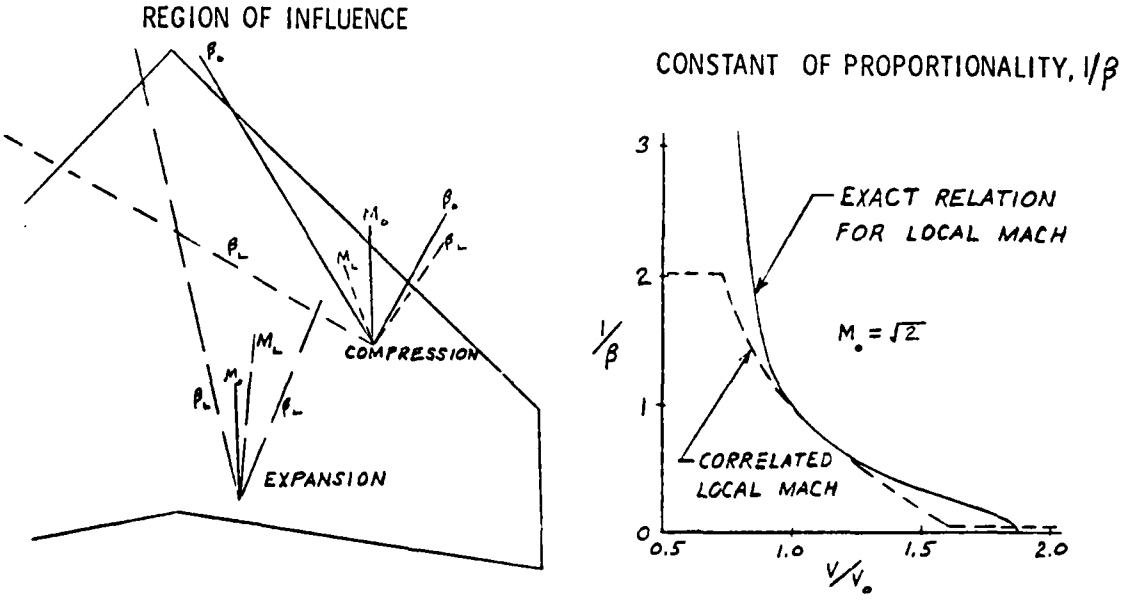

Fig. 2 Modification 2: local β

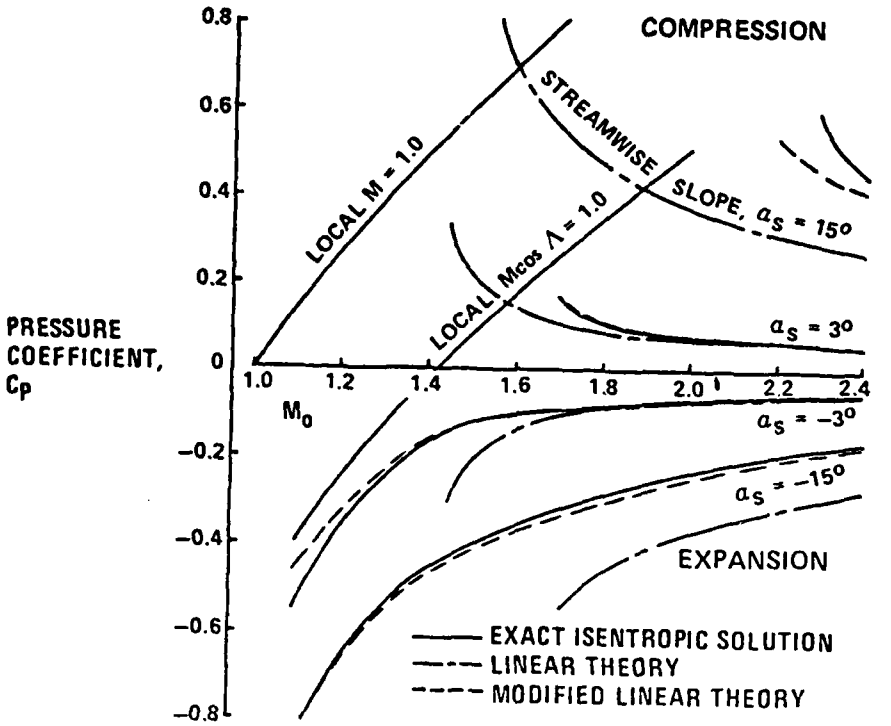

Fig. 3 45-deg swept ramp pressures.

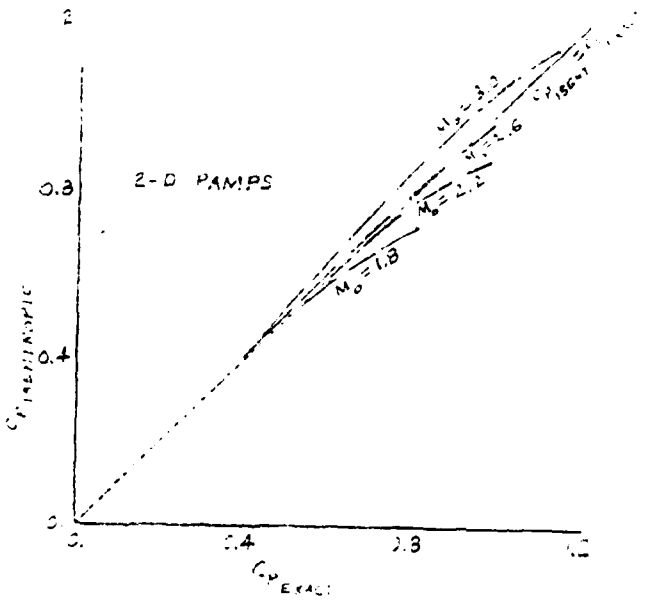

Fig. 4 Isentropic and exact ramp pressures.

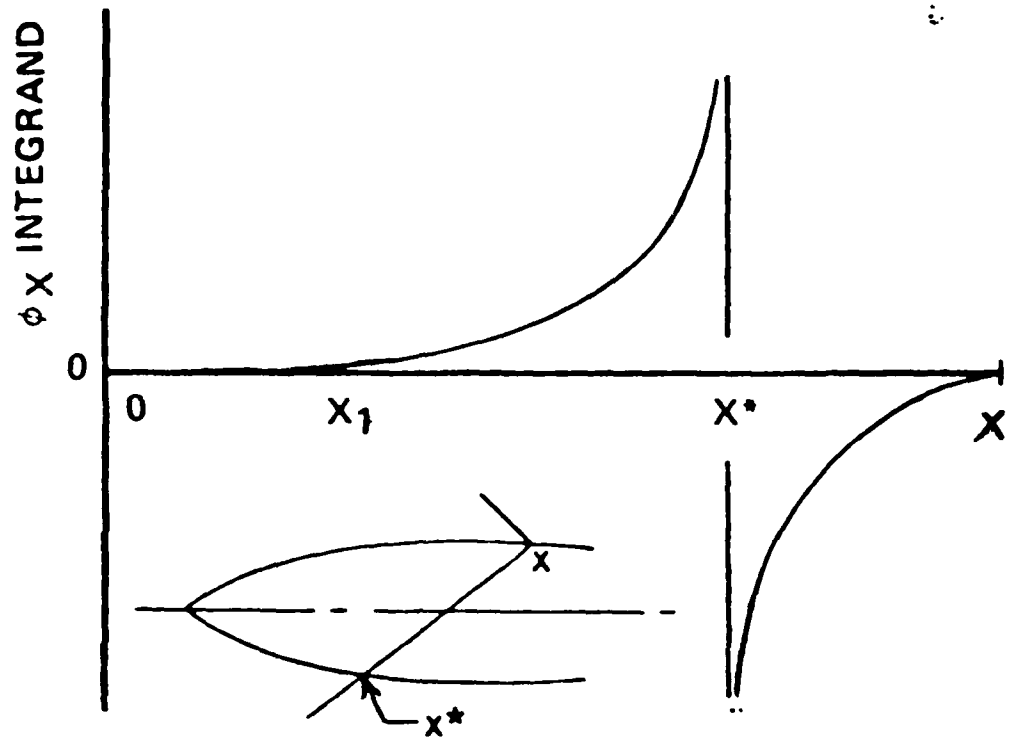

Fig. 5 Typical Integrand

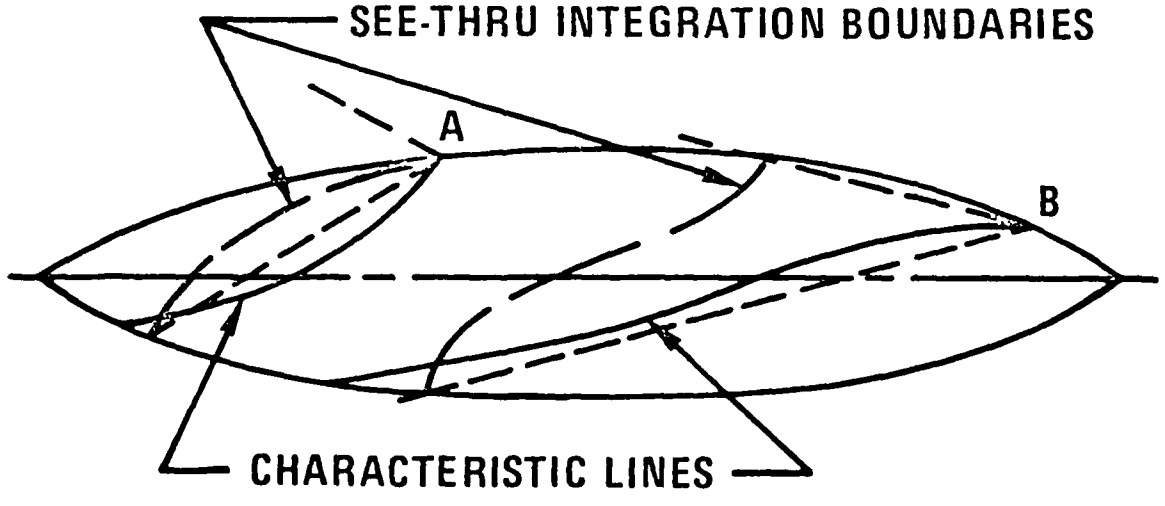

Fig. 6 Alternate Influencing Regions

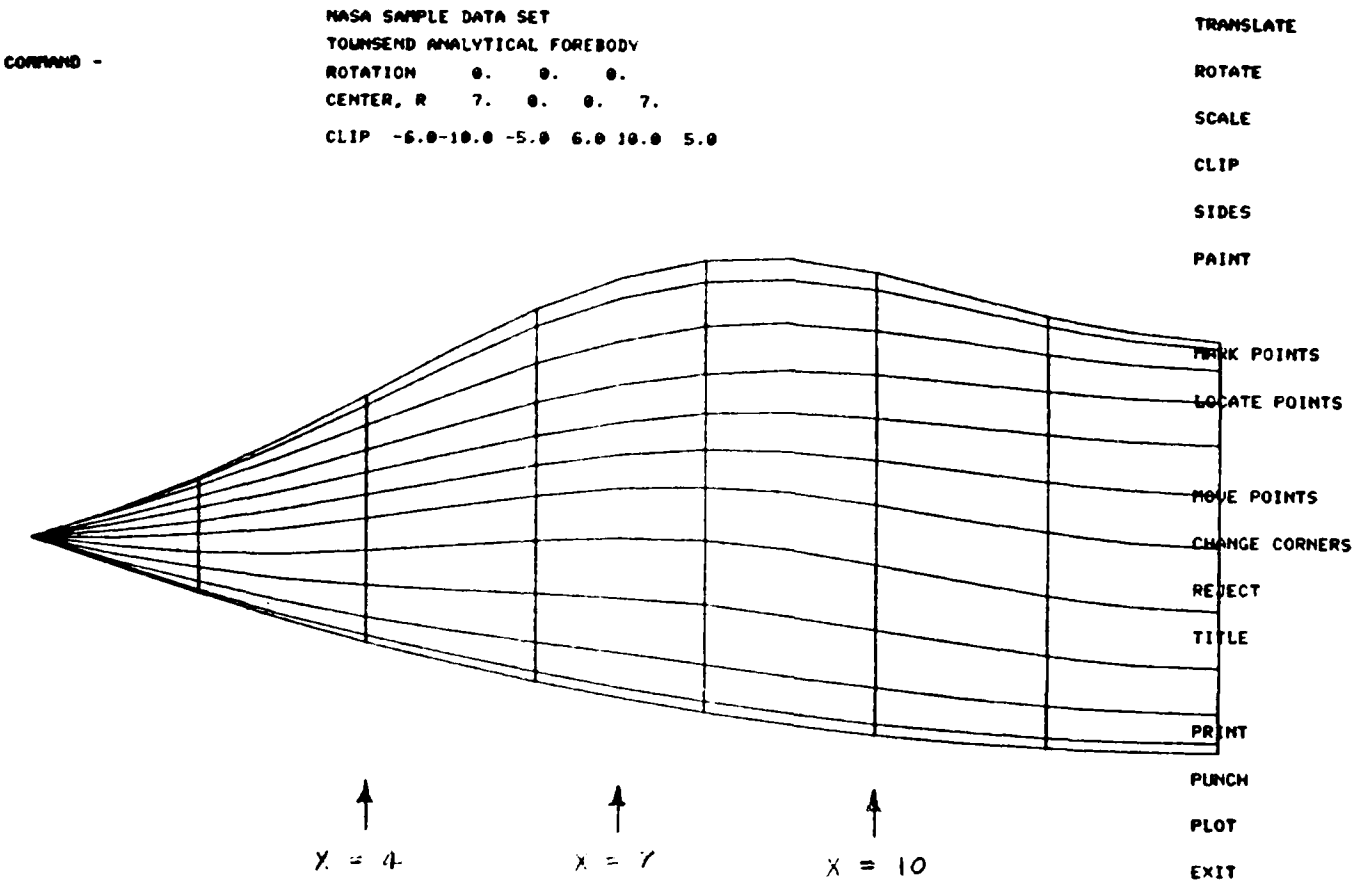

Figure 7 - Analytic Forebody Geometry

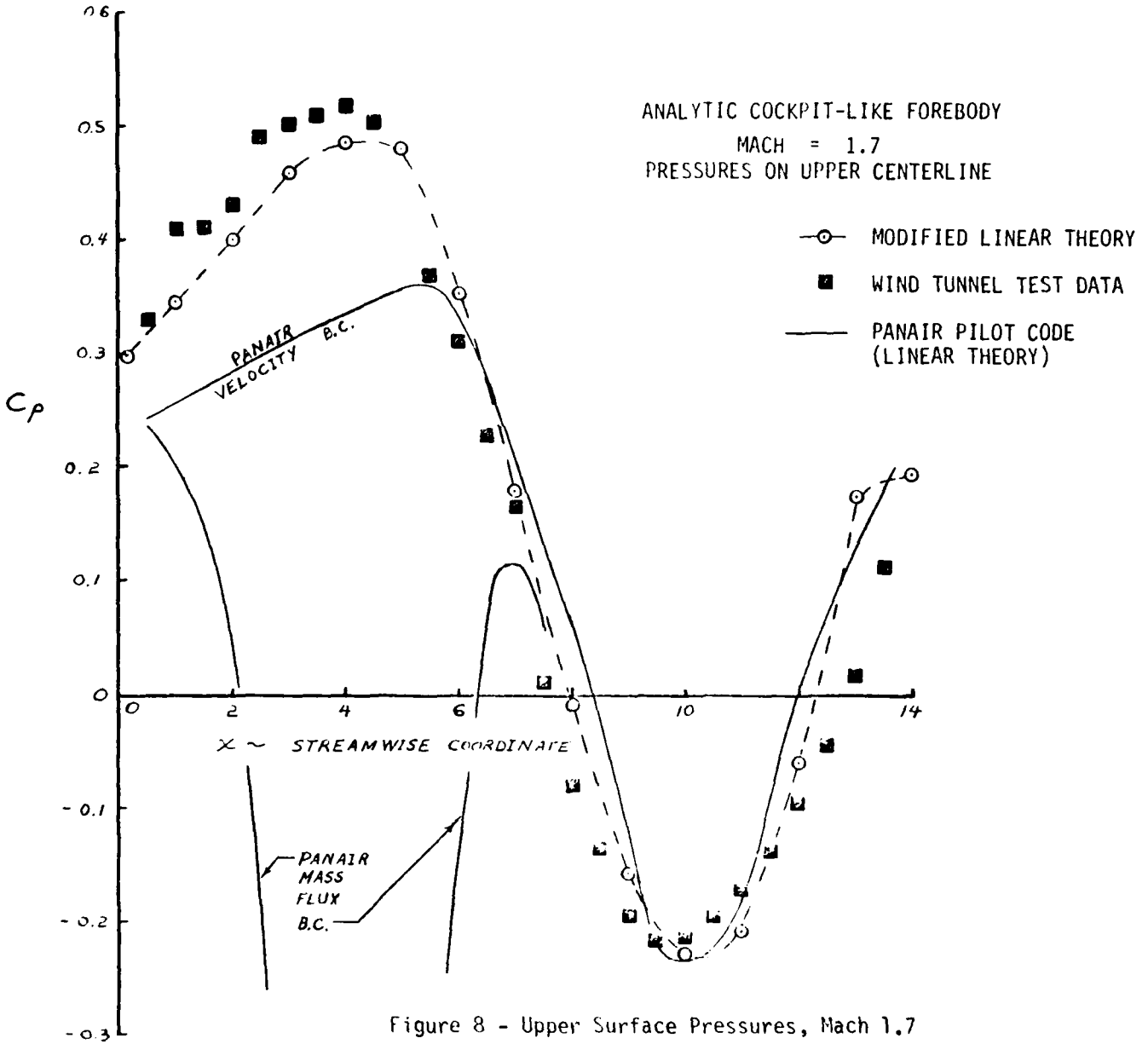

Figure 8 - Upper Surface Pressures, Mach 1.7

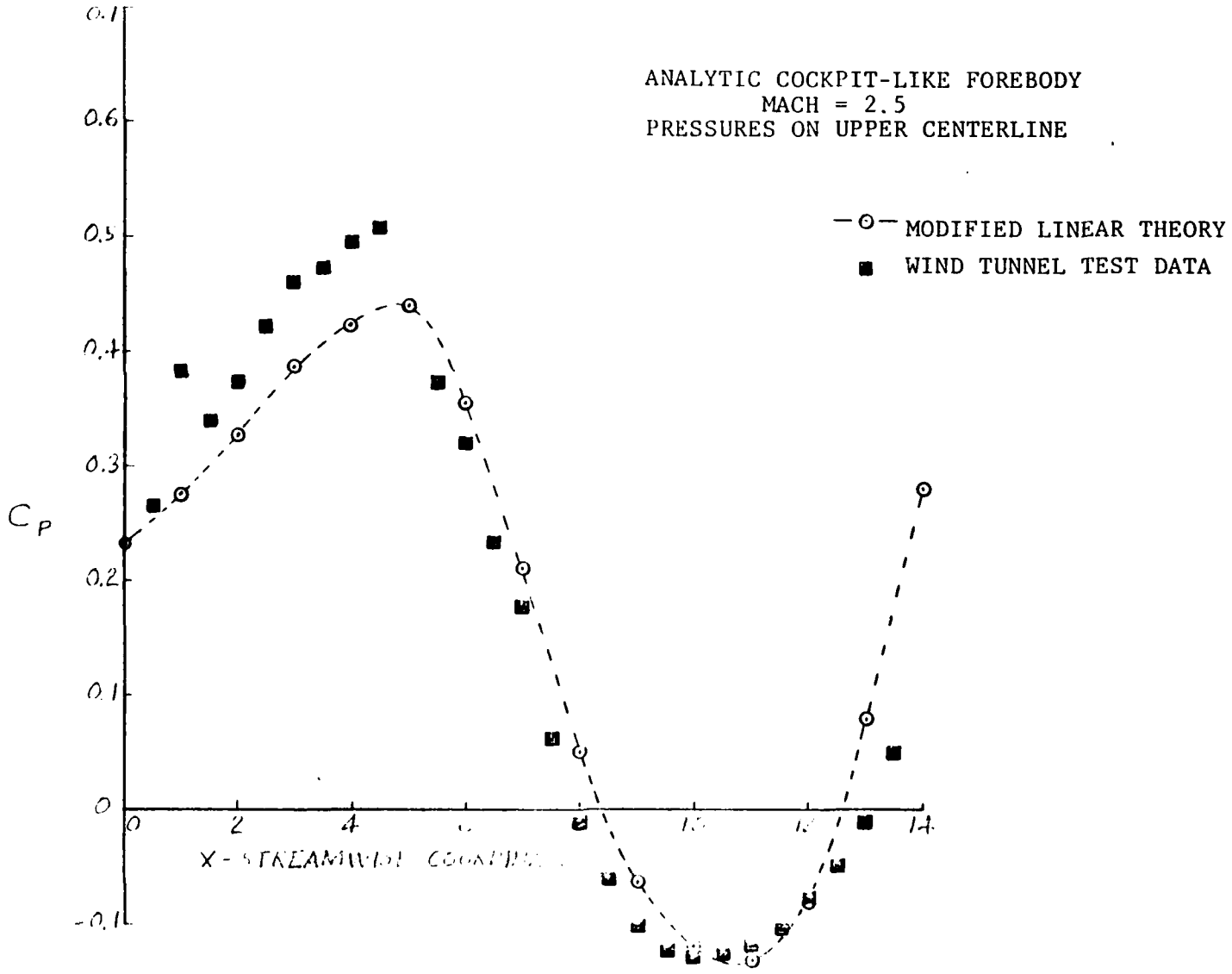

Figure 9 - Upper Surface Pressures, Mach 2.5

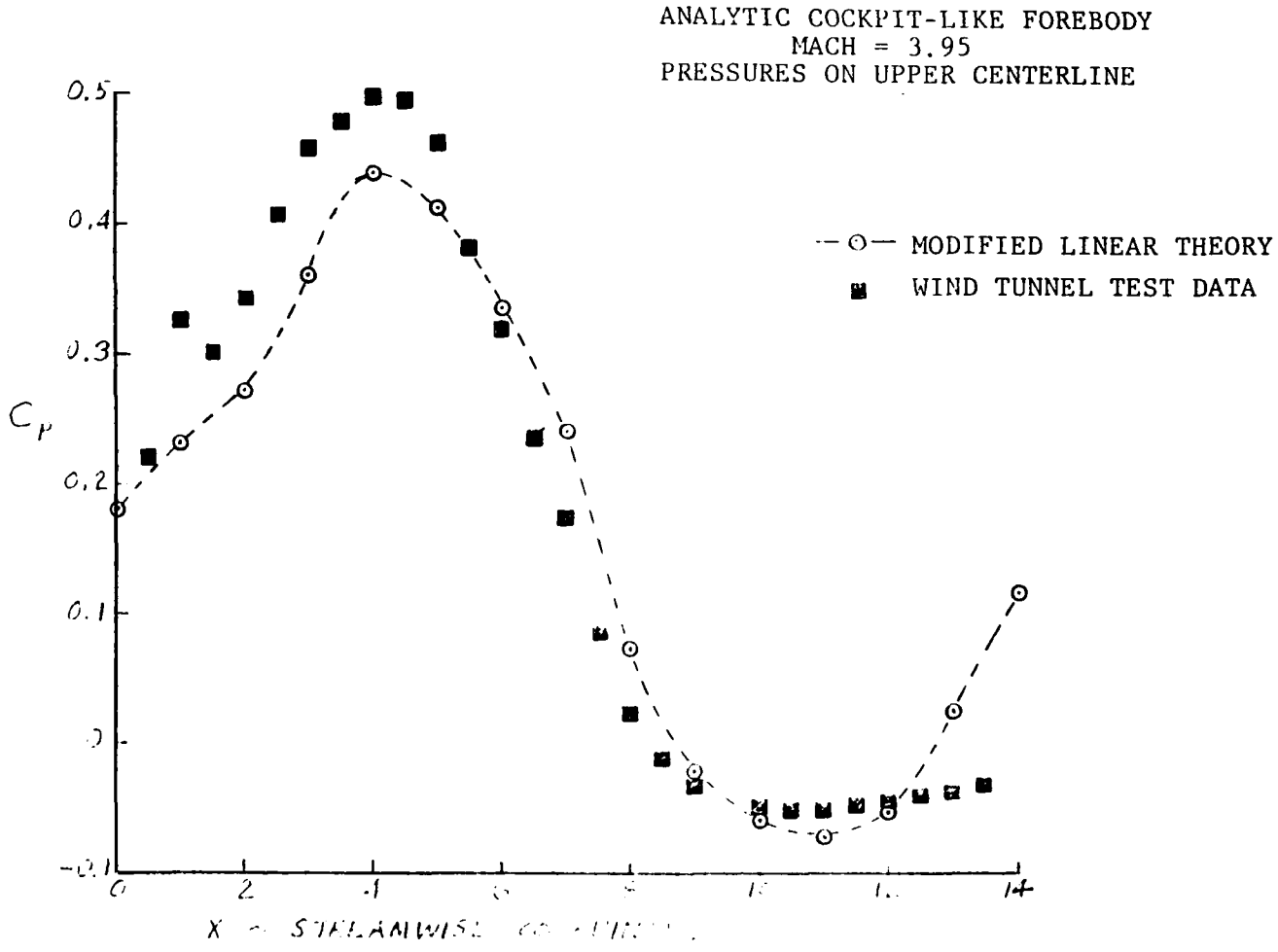

Figure 10 - Upper Surface Pressures, Mach 3.95

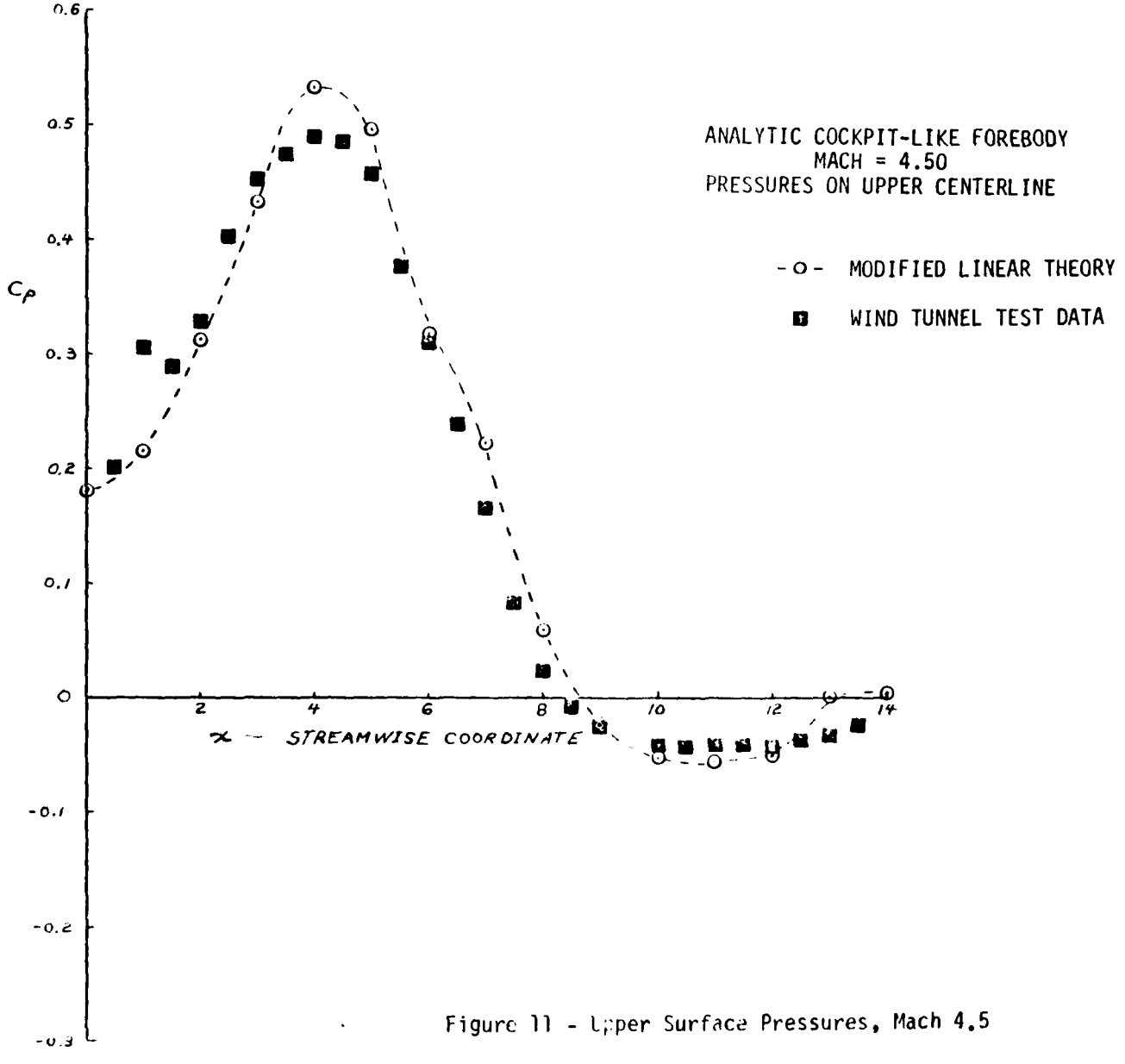

Figure 11 - Upper Surface Pressures, Mach 4.5

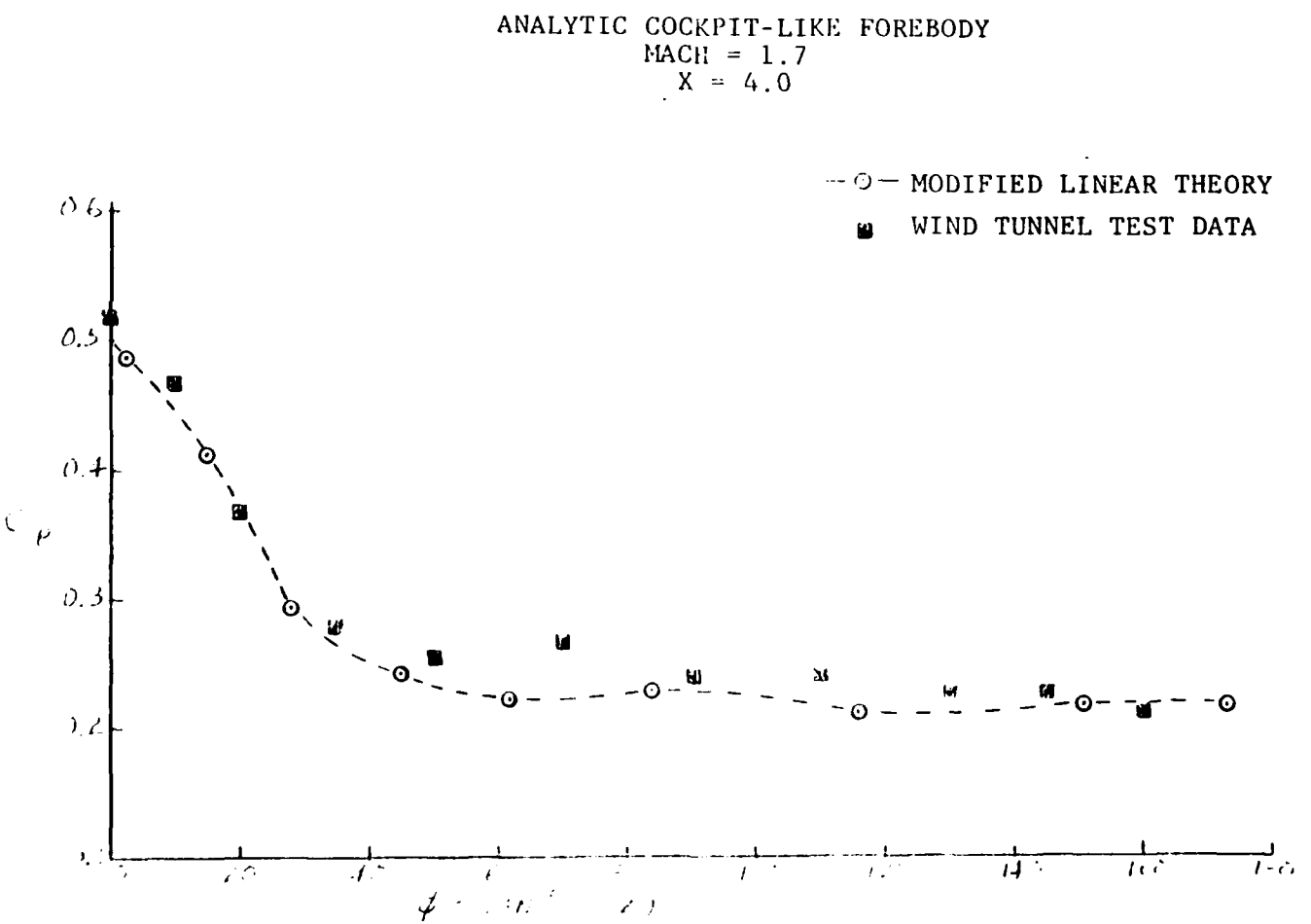

Figure 12 - Station Pressures, Mach 1.7, X = 4.0

ANALYTIC COCKPIT-LIKE FOREBODY
MACH = 1.7
X = 7.0

— ○ — MODIFIED LINEAR THEORY
■ WIND TUNNEL TEST DATA

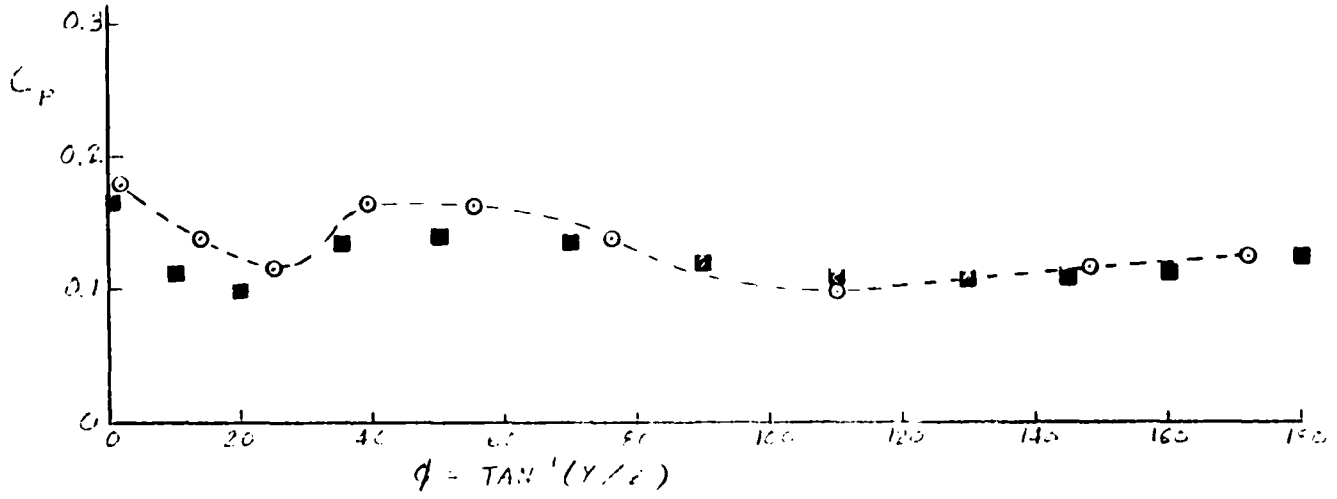

Figure 13 - Station Pressures, Mach 1.7, X = 7.0

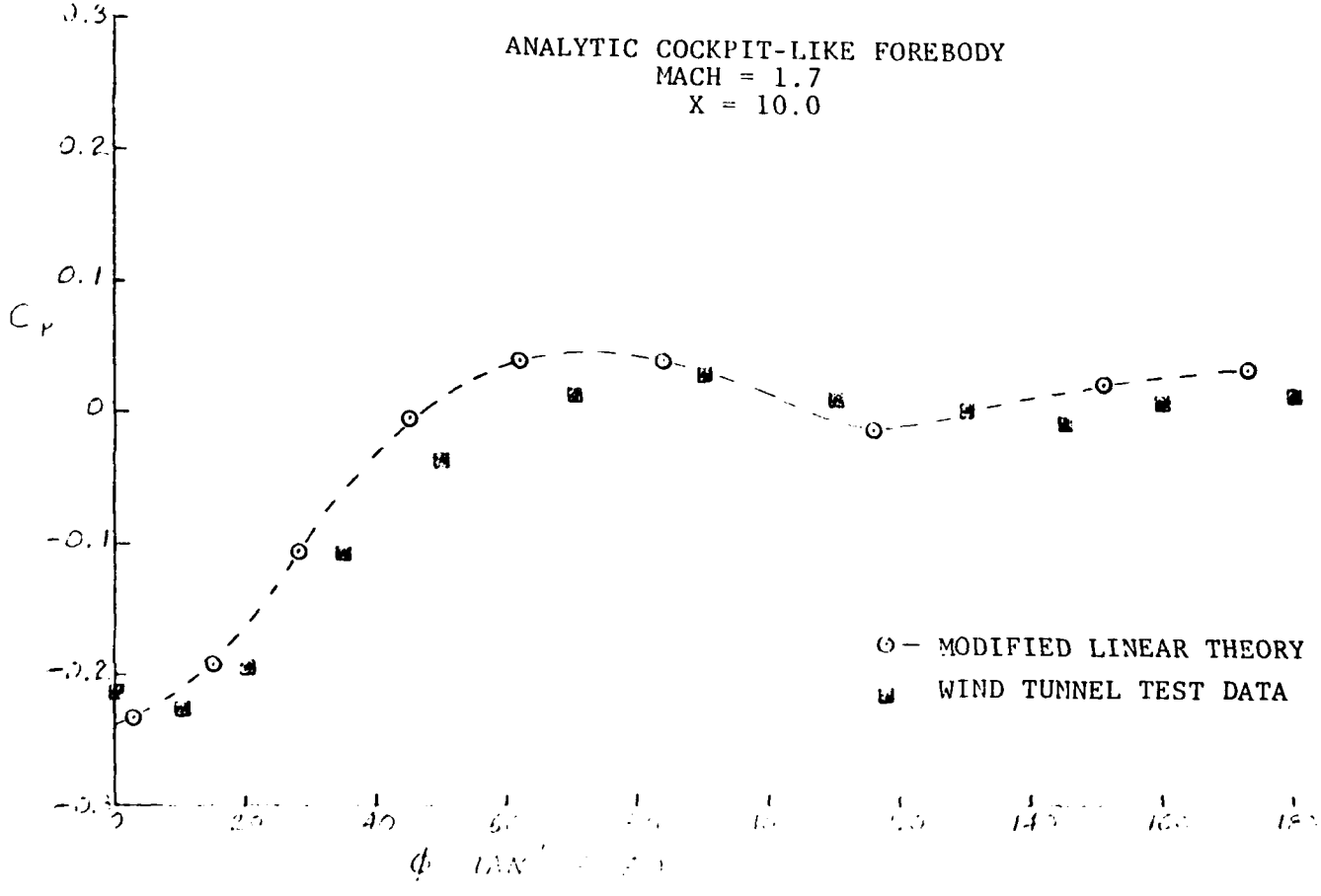

Figure 14 - Station Pressures, Mach 1.7, X = 10.0

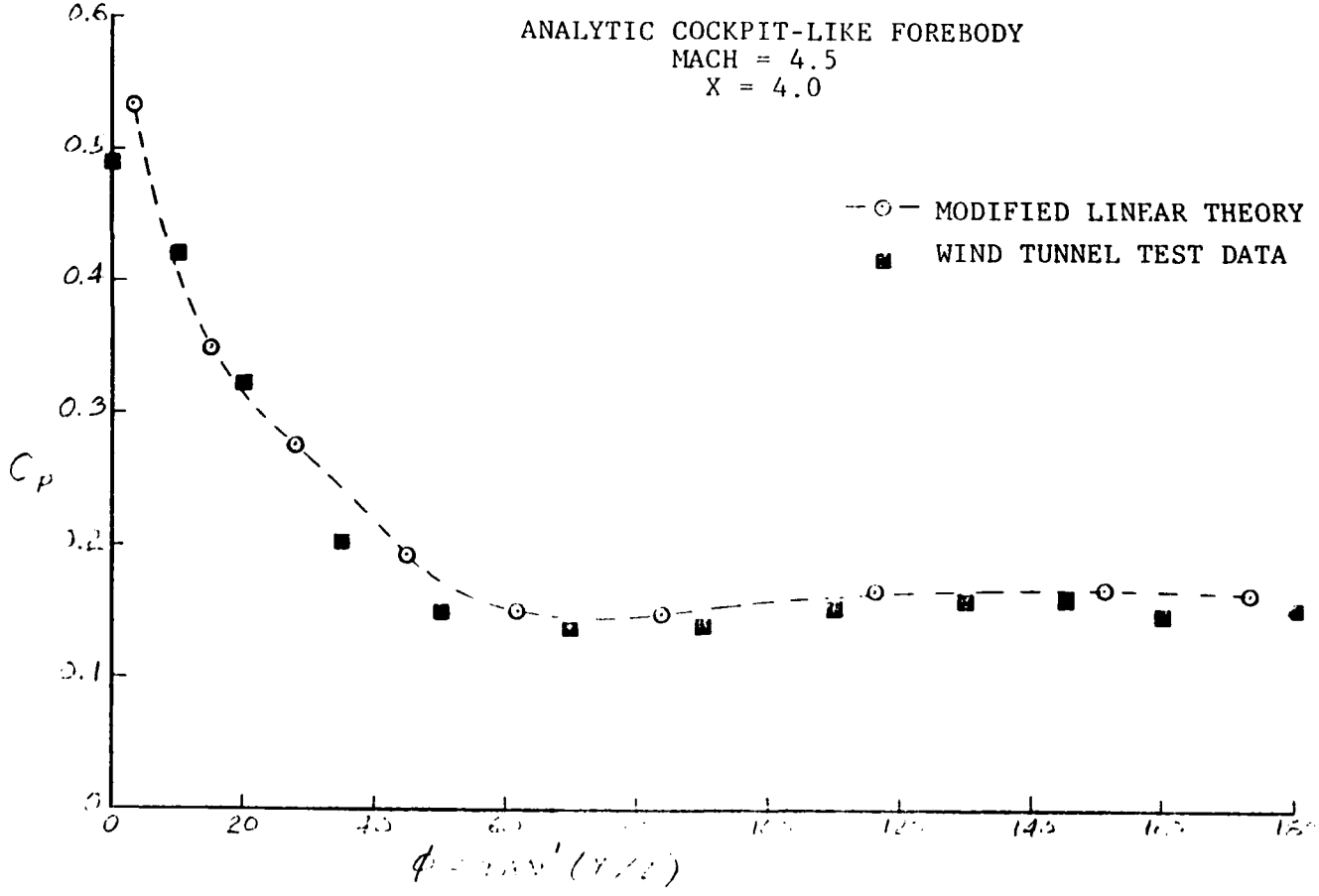

Figure 15 - Station Pressures, Mach 4.5, X = 4.0

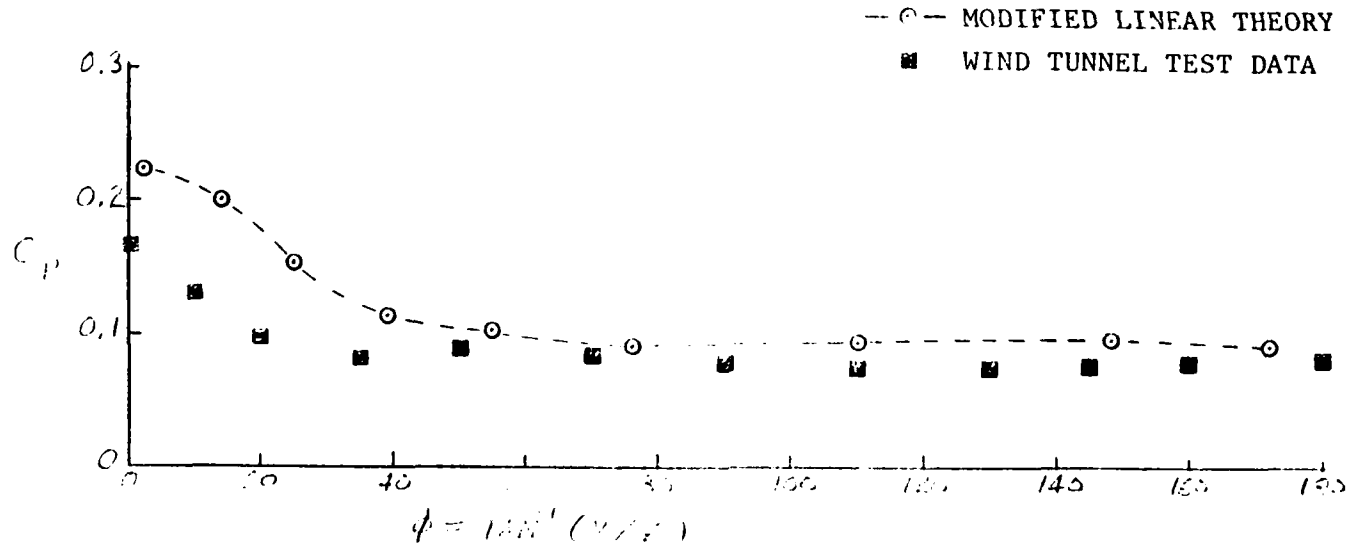

Figure 16 - Station Pressures, Mach 4.5, X = 7.0

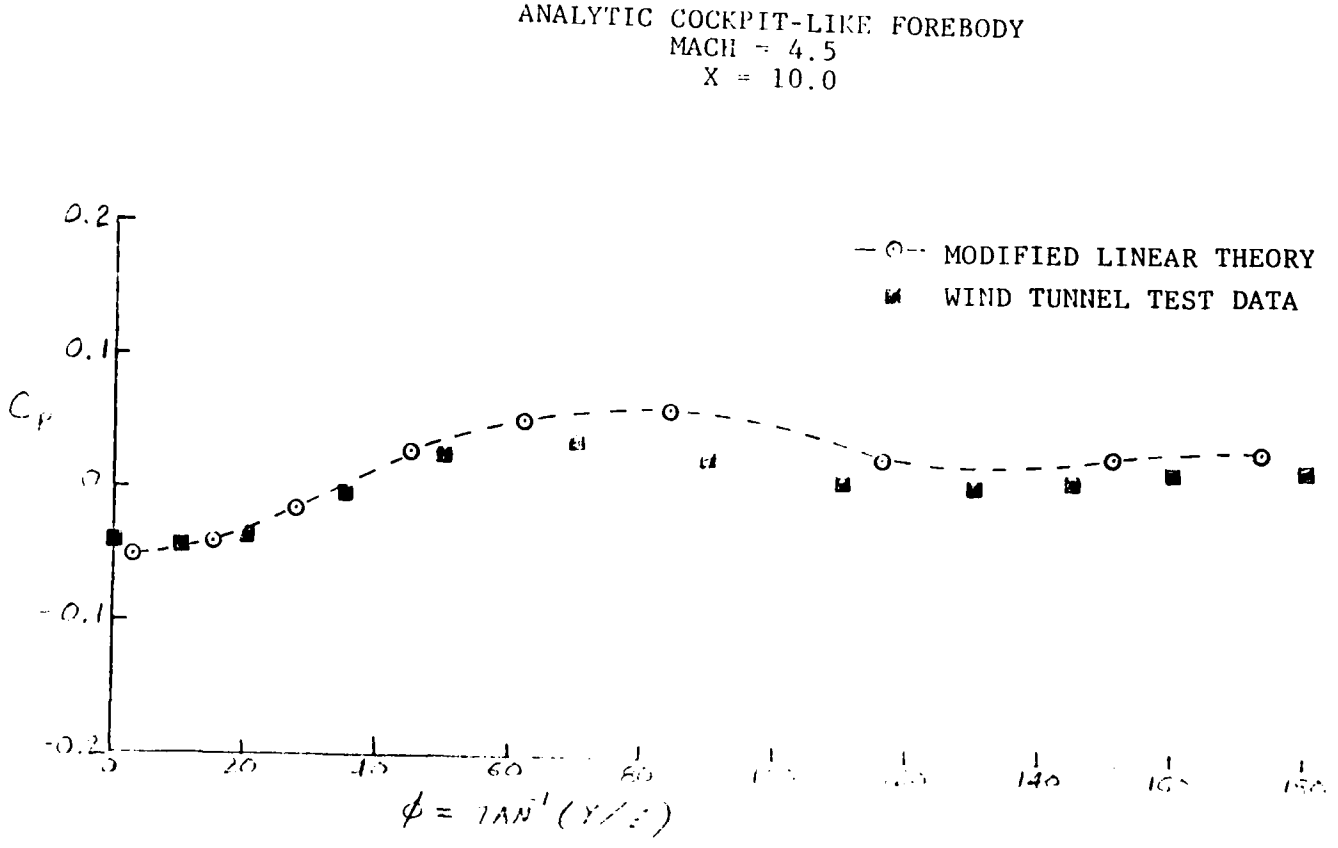

Figure 17 - Station Pressures, Mach 4.5, X = 10.0

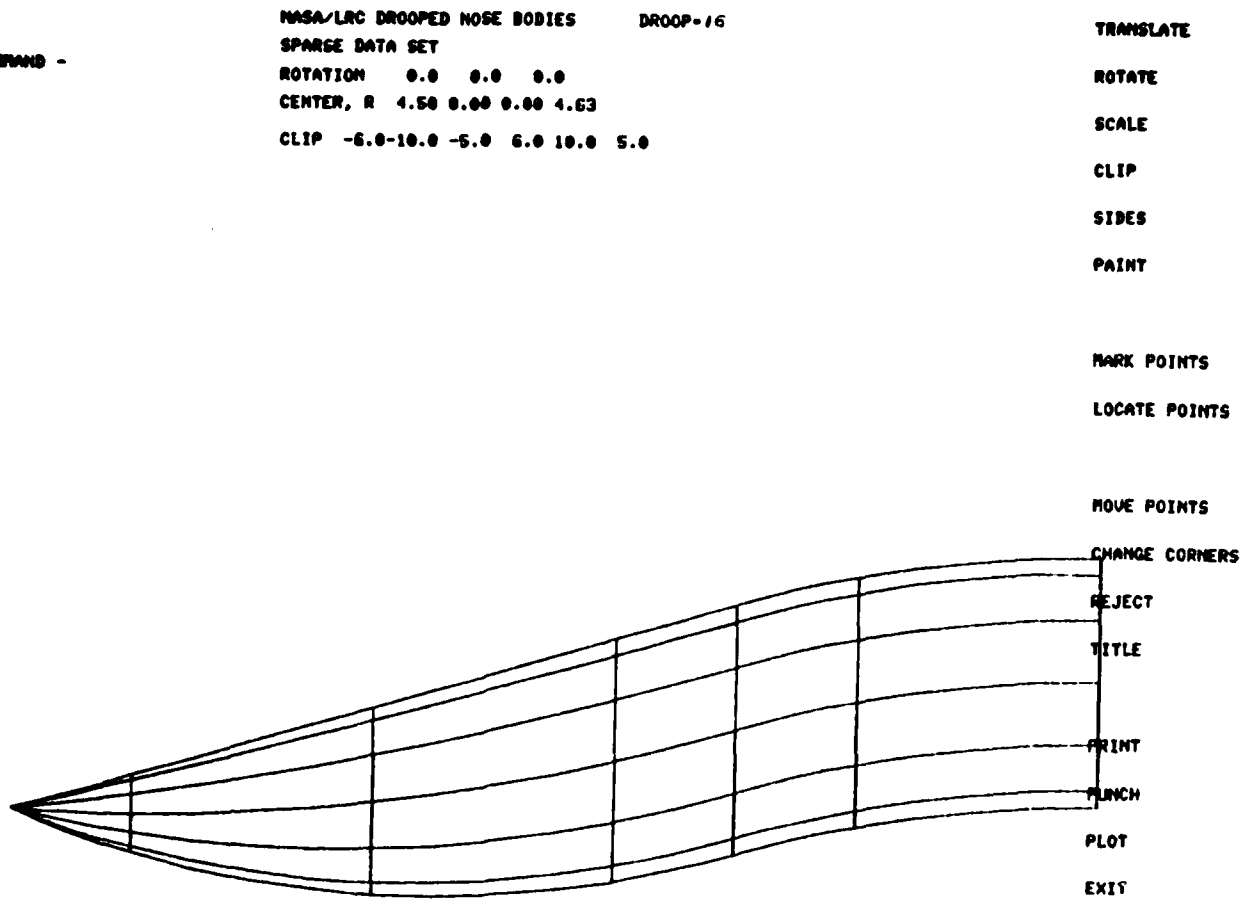

Figure 18 - 16^{O} Drooped Nose Body Shape

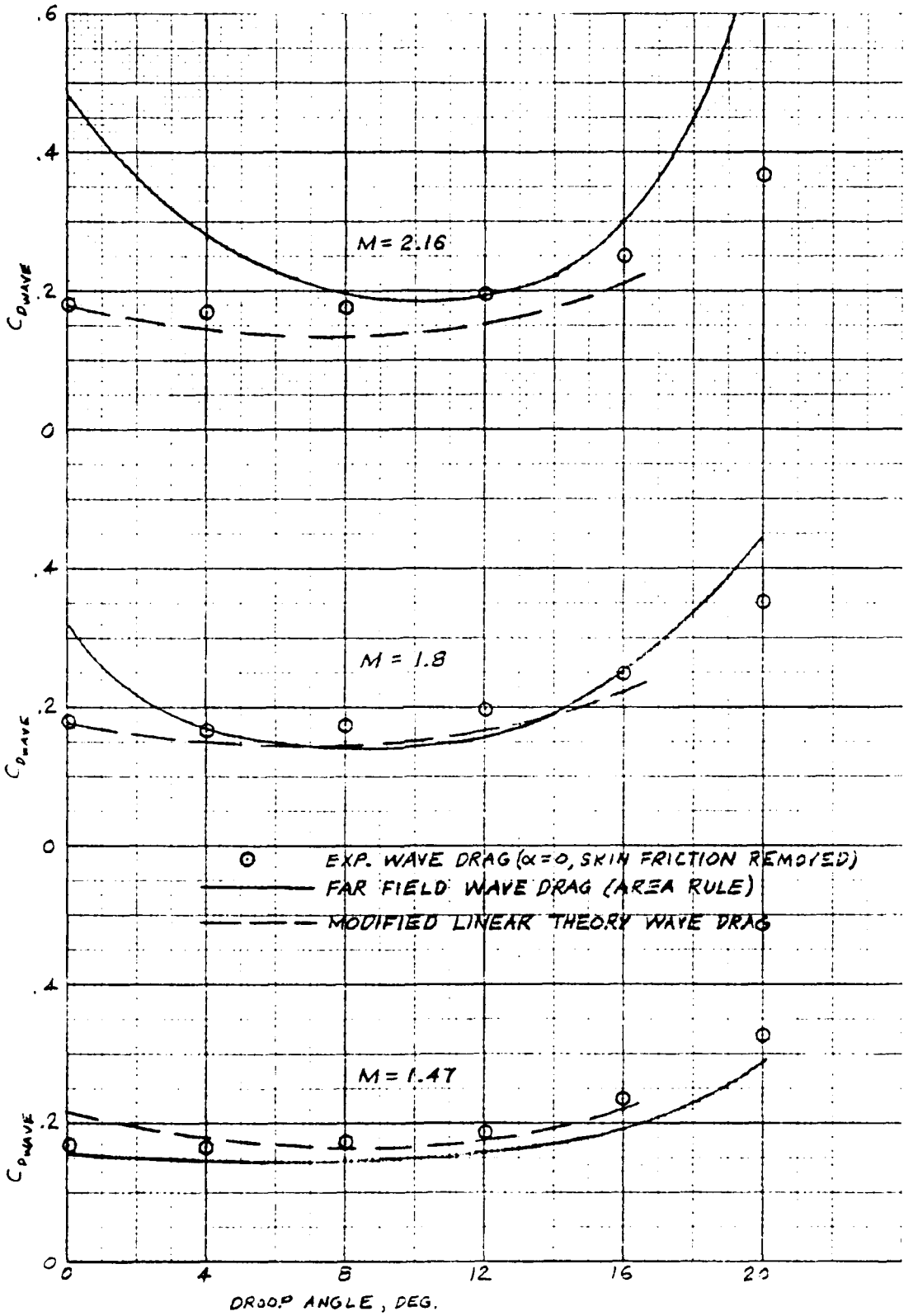

Figure 19 - Drooped Nose Body Drags

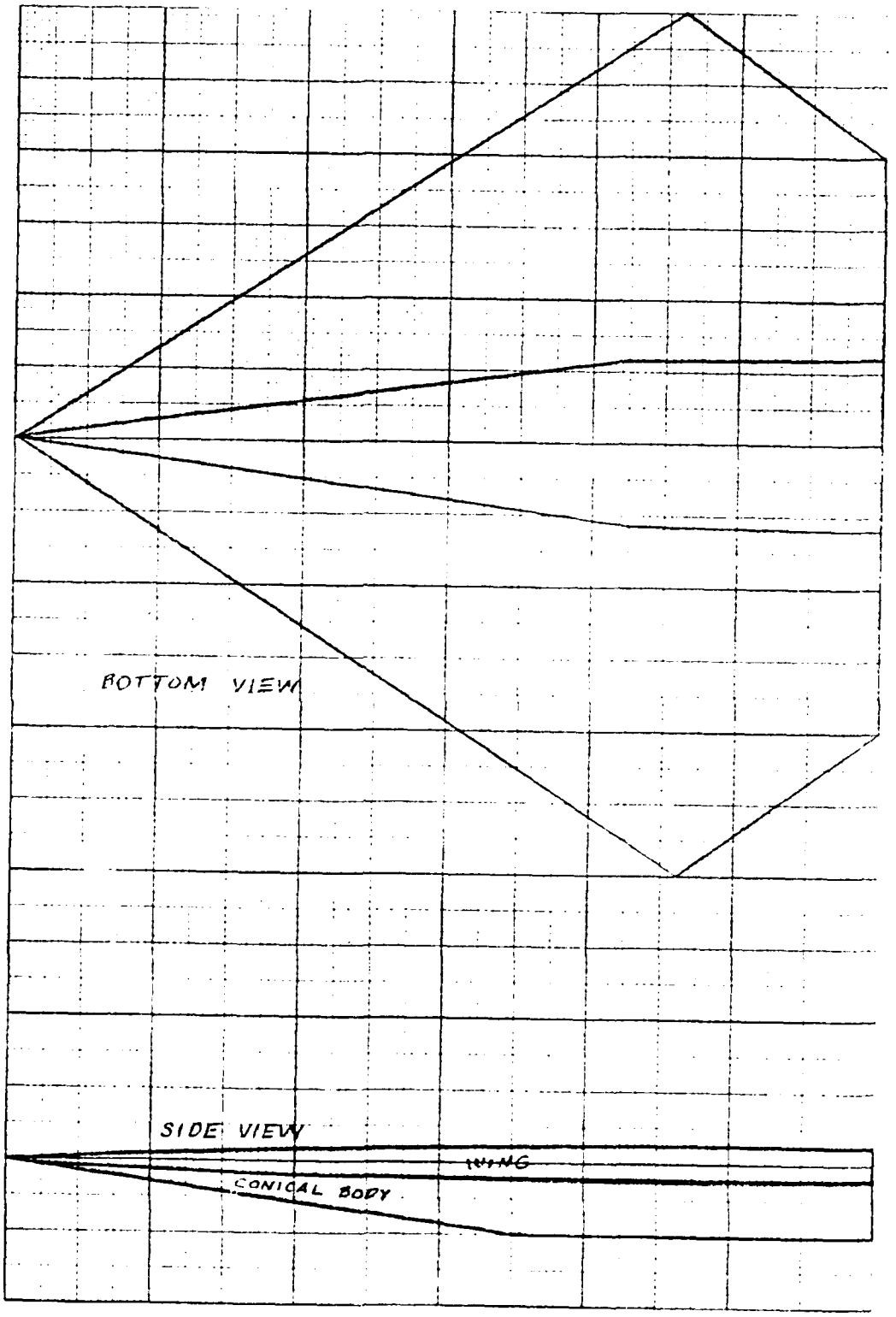

Figure 20 - Conical Wing Body Shape

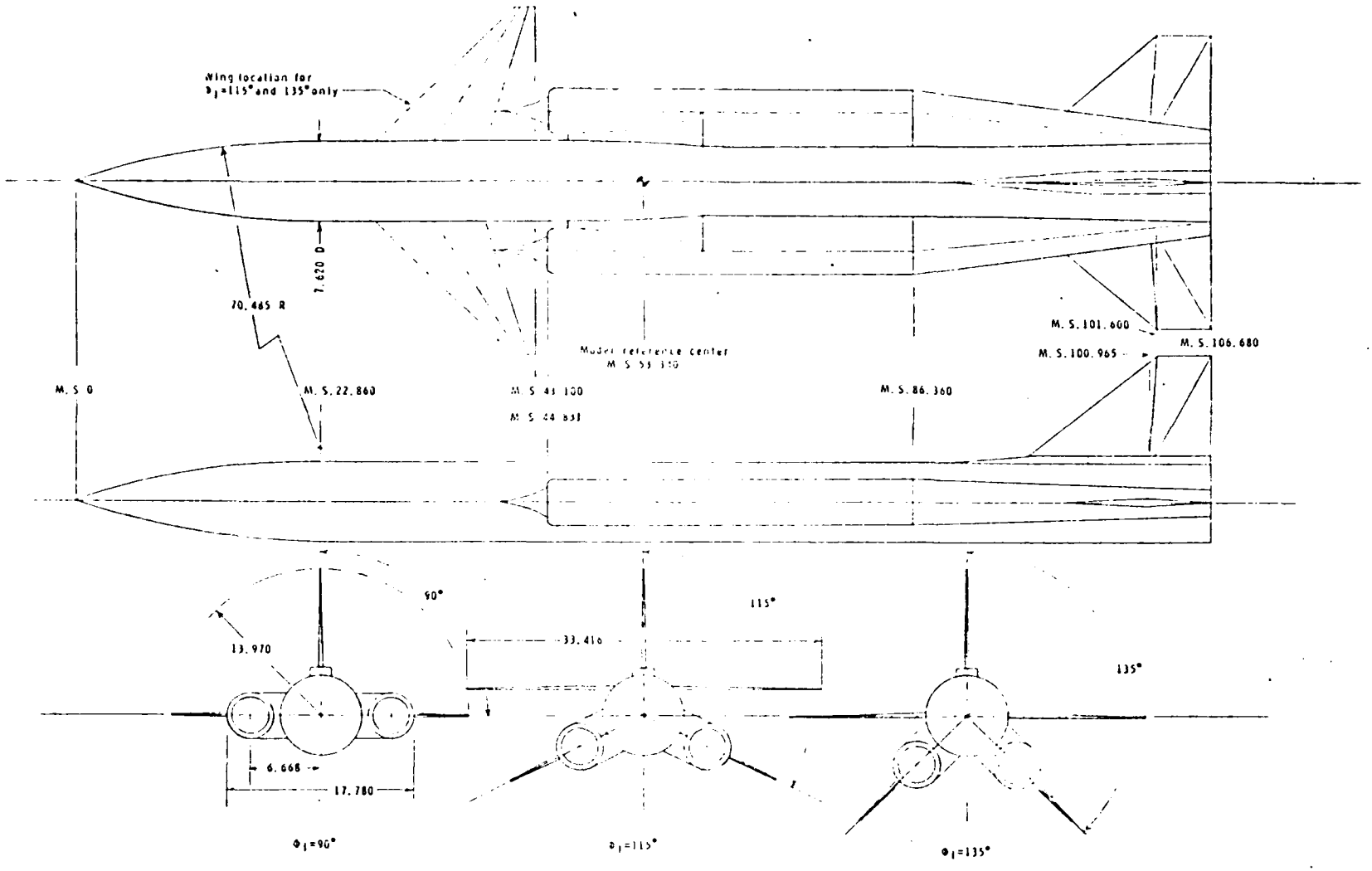

Figure 21 General arrangement of twin axis, symmetric inlet configuration. -Details of model. All dimensions are in centimeters unless otherwise noted.

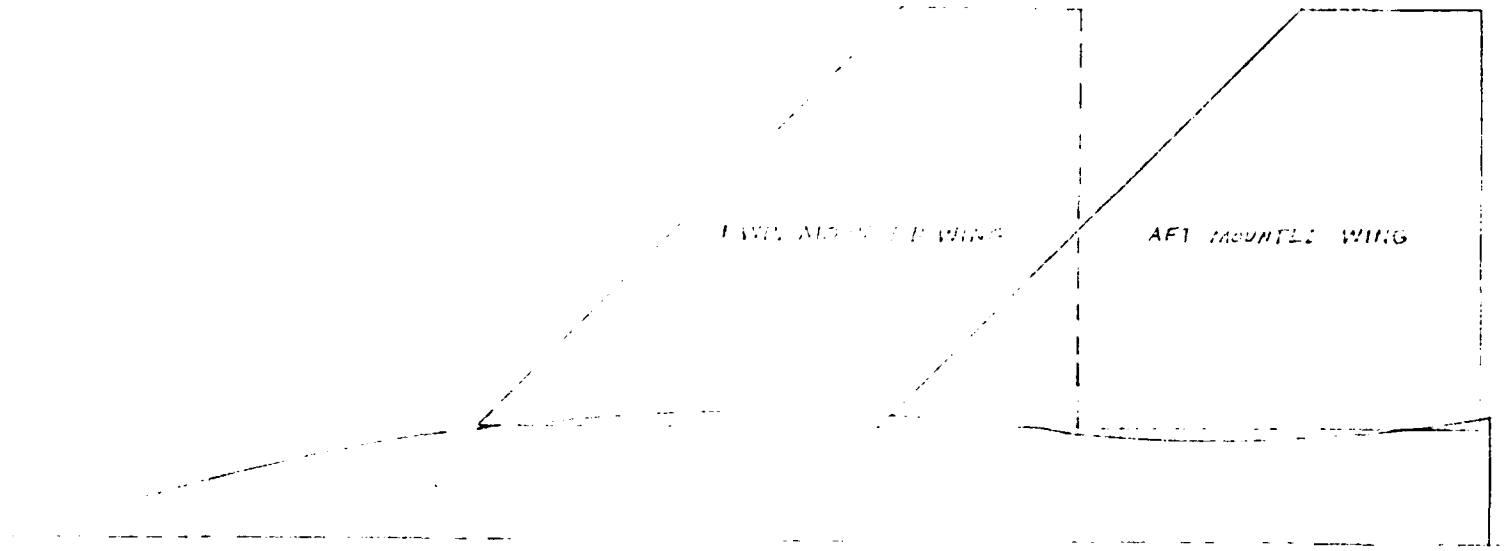

Figure 22 - Configuration for Area Rule Comparison Cases

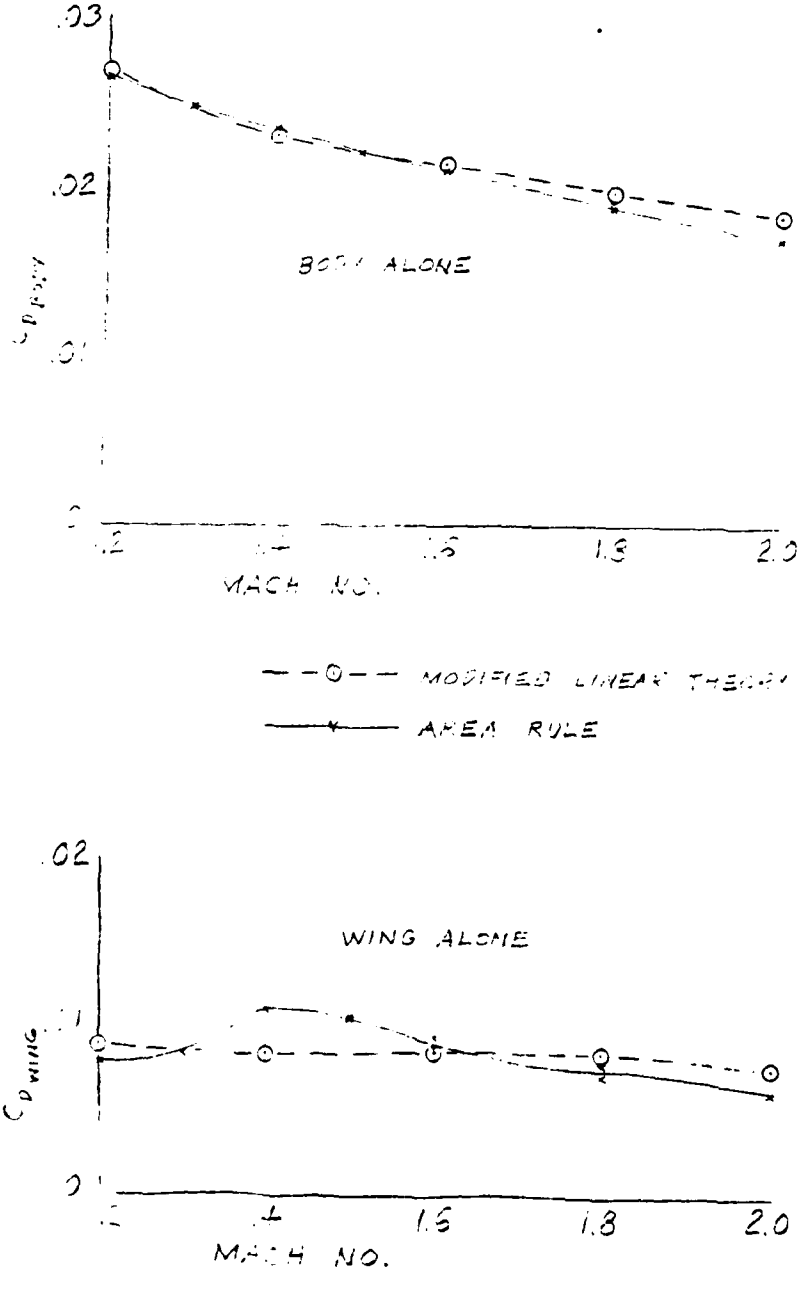

Figure 23 - Area Rule Comparison - Wing Alone and Body Alone Drags

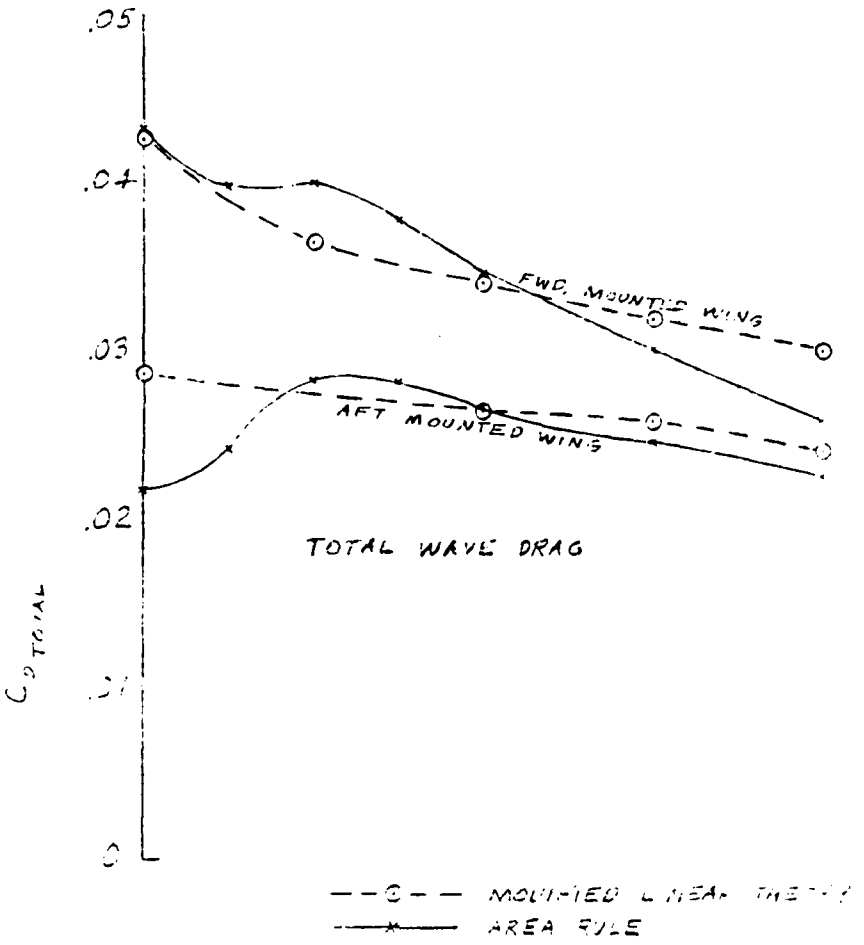

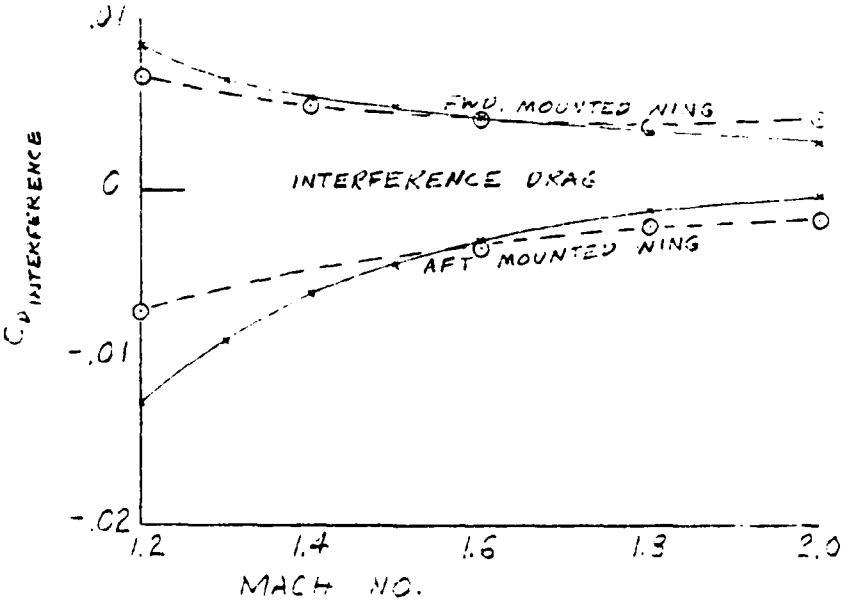

Figure 24 - Area Rule Comparison - Interference and Total Wave Drags

APPENDIX A

DERIVATION OF PERTURBATION VELOCITY EQUATIONS

A.1 Curved (Circular Arc) Panel with Source Strength Laterally Constant

The velocity potential is

$$\phi = -\frac{V_\infty}{\pi}\iint \frac{S(x_1)\,dx_1\,ds}{\sqrt{(x-x_1)^2-\beta^2(y-y_1)^2-\beta^2(z-z_1)^2}} \qquad (A-1)$$

where $ds = \sqrt{dy_1^2 + dz_1^2}$ on the surface of the panel. No subscript or a Q subscript (below) indicates the receiving point, and the subscript 1 indicates the sending point. $S(x_1)$ is the source strength at x_1. The curved panel is assumed to be a segment of a circle; thus with $ds = r_1\,d\mu$, $y_1 = r_1 \sin\mu$ and $z_1 = r_1 \cos\mu$ we have

$$\phi = -\frac{V_\infty}{\pi}\int\int \frac{r_1\,S(x_1)\,dx_1\,d\mu}{\sqrt{(x-x_1)^2-\beta^2(y-r_1\sin\mu)^2-\beta^2(z-r_1\cos\mu)^2}} \qquad (A-2)$$

where y and z must be defined relative to the center of the circular arc panel segment. On any panel, the curvature and (y,z) coordinates of the arc center can vary with x. The angle μ is positive clockwise and r_1 is defined as positive for convex panels and negative for concave panels. We will integrate from left to right, so $r_1\,d\mu$ will be positive for both convex and concave panels. Now if we let $y = 0$, the $\mu = 0$ direction is defined by the vector from the center to (0,z) for convex panels, and the opposite direction for concave panels (i.e., from the receiving point to the center of the panel arc). Also define r_Q as the vector length from the circular arc center to the receiving point, but with the same sign as r_1. Now

$$\phi = -\frac{V_\infty}{\pi}\int r_1 S(x_1)\,dx_1 \int \frac{d\mu}{\sqrt{(x-x_1)^2-\beta^2 r_1^2\sin^2\mu-\beta^2(r_Q-r_1\cos\mu)^2}}$$

$$= -\frac{V_\infty}{\pi}\int r_1 S(x_1)\,dx_1 \int \frac{d\mu}{\sqrt{(x-x_1)^2-\beta^2 r_Q^2-\beta^2 r_1^2+2\beta^2 r_Q r_1\cos\mu}} \qquad (A-3)$$

Transforming $\mu = 2\psi$, $d\mu = 2\,d\psi$, $\cos\mu = 1 - 2\sin^2\psi$,

$$\phi = -\frac{2V_\infty}{\pi}\int r_1 S(x_1)\,dx_1 \int \frac{d\psi}{\sqrt{(x-x_1)^2-\beta^2(r_Q-r_1)^2-4\beta^2 r_Q r_1\sin^2\psi}}$$

$$= -\frac{2V_\infty}{\pi}\frac{\int r_1 S(x_1)\,dx_1}{\sqrt{(x-x_1)^2-\beta^2(r_Q-r_1)^2}} \int \frac{d\psi}{\sqrt{1-\frac{4 r_Q r_1\sin^2\psi}{\left(\frac{x-x_1}{\beta}\right)^2-(r_Q-r_1)^2}}} \qquad (A-4)$$

In Eq. (A-4), if $k_1 \leq 1$, the inner integral is an elliptic integral of the first kind with modulus

$$k_1 = \sqrt{\frac{4 r_Q r_1}{\left(\frac{x - x_1}{\beta}\right)^2 - (r_Q - r_1)^2}} \qquad (A-5)$$

and $k_1 \leq 1$ when $x_1 \leq x^*$, where x^* is defined as the x_1 where the forecone passes through the opposite side of the (imaginary) complete circle defined by the radius of the panel element being considered, or

$$x^* = x - \beta \left| r_Q + r_{x^*} \right| \qquad (A-6)$$

For $x > x^*$, we must transform again using $\sin \omega = k_1 \sin \psi$. This gives:

$$\phi = -\frac{2 V_0}{\pi} \int_0^{x^*} \frac{r_1 S(x_1)\, dx_1}{\beta \sqrt{\left(\frac{x - x_1}{\beta}\right)^2 - (r_Q - r_1)^2}} \int_{\psi_R}^{\pi/2} \frac{d\psi}{\sqrt{1 - k_1^2 \sin^2 \psi}}$$

$$- \frac{2 V_0}{\pi} \int_{x^*}^{x_c} \frac{r_1 S(x_1)\, dx_1}{\beta \sqrt{\left(\frac{x - x_1}{\beta}\right)^2 - (r_Q - r_1)^2}} \int_{\omega_L}^{\omega_R} \frac{\cos \omega\, d\omega}{k_1 \cos \psi \sqrt{1 - k_1^2 \sin^2 \omega}} \qquad (A-7)$$

For the last transformation to be single-valued, we must limit $-\pi/2 \leq \omega \leq \pi/2$ ($-\pi < \mu < \pi$). Then $\cos \omega = \sqrt{1 - \sin^2 \omega}$ and $\cos \psi = \sqrt{1 - (k_1 \sin \omega)^2}$

Defining $k_2 = 1/k_1$, we have:

$$\phi = -\frac{2 V_0}{\pi} \int_0^{x^*} \frac{r_1 S(x_1)\, dx_1}{\beta \sqrt{\left(\frac{x - x_1}{\beta}\right)^2 - (r_Q - r_1)^2}} \left[F\{k_1, \omega_R\} - F\{k_1, \omega_L\} \right]$$

$$- \frac{2 V_0}{\pi} \int_{x^*}^{x_c} \frac{r_1 S(x_1)\, dx_1}{\beta \sqrt{1 \; r_Q r_1}} \left[F\{k_2, \omega_R\} - F\{k_2, \omega_L\} \right] \qquad (A-8)$$

where to include the complete area of integration, the bracketed terms in Eq. (A-8) must be summed over all the panels within the area of integration defined by the characteristics. Also, except for bodies of revolution, x^* will be different for each panel.

The next step is to differentiate with respect to x, y and z to obtain the perturbation velocities. The y derivative will be taken first because it is

simpler and is the same for $x_1 < x^*$ and $x_1 > x^*$. Going back to Eq. (A-4), the only terms that are functions of y are the limits of integration on ψ when not on a characteristic, and then

$$\frac{\partial \psi}{\partial y} = \frac{1}{2}\frac{\partial \mu}{\partial y} = -\frac{1}{2\pi_Q} \tag{A-9}$$

The y derivative of Eq. (A-4) can be written in several forms:

$$\phi_y = \frac{V_\infty}{\pi}\int_{x_0}^{x_c} \frac{\pi_1 S(x_1)}{\beta \pi_Q}\left[\frac{1}{\sqrt{\left(\frac{x-x_1}{\beta}\right)^2 - (\pi_Q - \pi_1)^2 - 4\pi_Q\pi_1 \sin^2\psi}}\right]_{-\psi_L}^{\psi_R} dx_1$$

$$= \frac{V_\infty}{\pi}\int_{x_0}^{x_c} \frac{\pi_1 S(x_1)}{\beta \pi_Q \sqrt{\left(\frac{x-x_1}{\beta}\right)^2 - (\pi_Q - \pi_1)^2}}\left[\frac{1}{\sqrt{1 - \frac{4\pi_Q\pi_1}{\left(\frac{x-x_1}{\beta}\right)^2 - (\pi_Q-\pi_1)^2}\sin^2\psi}}\right]_{-\psi_L}^{\psi_R} dx_1$$

$$= \frac{V_\infty}{\pi}\int_{x_0}^{x_c} \frac{\pi_1 S(x_1)}{\beta \pi_Q \sqrt{\left(\frac{x-x_1}{\beta}\right)^2 - (\pi_Q - \pi_1)^2}}\left[\frac{1}{\sqrt{1 - k^2\sin^2\psi}}\right]_{-\psi_L}^{\psi_R} dx_1$$

but if either lateral limit is on a characteristic, set that term to zero because on a characteristic

$$\frac{\partial \psi}{\partial y} = \frac{\partial \mu}{\partial y} = 0$$

For the x and z derivatives, we will need to take derivatives of the limits of integration. The upper limit (x_c or x_1) of x integration is, in the vicinity of a point A on the surface of the body where ϵ is the local slope,

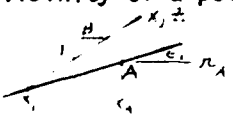

$$x_1 = \frac{x - x_A\beta\epsilon_1 - \beta(z - r_A)}{1 - \beta\epsilon_1} \tag{A-11}$$

where $r_1 \approx r_A + \epsilon_1 (x - x_A)$. Therefore,

$$\frac{\partial x_1}{\partial x} = \frac{1}{1 - \beta\epsilon}$$

$$\frac{\partial x_1}{\partial z} = -\frac{\beta}{1 - \beta\epsilon} \tag{A-12}$$

The lateral limits, when $x < x^*$, are functions of ψ or μ which are independent of x and z, so

$$\frac{\partial \psi}{\partial x} = \frac{\partial \psi}{\partial z} = 0 \qquad \text{when} \quad x < x^* \tag{A-13}$$

When $x > x^*$, the ω transformation is such that on the forecone (characteristic), $\omega = \pm \pi/2$. Thus,

$$\frac{\partial \omega}{\partial x} = \frac{\partial \omega}{\partial z} = 0 \qquad \text{for } x > x^*, \text{ on a characteristic} \tag{A-14}$$

But with $x > x^*$ and the lateral limit not on a characteristic, from $\sin \omega = k_1 \sin \psi$ we derive

$$\frac{\partial \omega}{\partial x} = \frac{\sin \psi}{\cos \omega} \frac{\partial k_1}{\partial x}$$

$$\frac{\partial \omega}{\partial z} = \frac{\sin \psi}{\cos \omega} \frac{\partial k_1}{\partial z} = \frac{\sin \psi}{\cos \omega} \frac{\partial k_1}{\partial \eta_2} \qquad (x > x^*, \text{ not on a characteristic}) \tag{A-15}$$

where

$$\frac{\partial k_1}{\partial x} = -\frac{2\sqrt{\eta_2 \eta_1}\,(x - x_1)}{\beta^2 \left[\left(\frac{x - x_1}{\beta}\right)^2 - (\eta_2 - \eta_1)^2\right]^{3/2}}$$

$$\frac{\partial k_1}{\partial \eta_2} = \frac{\sqrt{\frac{\eta_1}{\eta_2}}\left[\left(\frac{x - x_1}{\beta}\right)^2 + \eta_2^2 - \eta_1^2\right]}{\left[\left(\frac{x - x_1}{\beta}\right)^2 - (\eta_2 - \eta_1)^2\right]^{3/2}} \tag{A-16}$$

Now we are ready to differentiate Eq. (A-8) in three parts: (1) the derivative of the upper limit on the x integration, (2) the derivative of the lateral limits of integration, and (3) the derivative of the integrand. A contribution to part (1) occurs at $x_c = x$ when the receiving point is on the surface of the body, and also whenever there is a local maximum of the integration variable x_1 due to the forecone from the receiving point tracing directly to the body (panel) at a right angle. At these points, $k_2 = 0$ and $F(0, \pm \pi/2) - F(0, \mp \pi/2) = \mp \pi$, with the sign determined by the sign of r_1. So differentiating the upper limit of Eq. (A-8) and substituting Eqs. (A-12),

$$\phi_{x_1} = -\frac{V_0 S(x_1)}{\beta} \sqrt{\frac{\eta_1}{\eta_2}} \frac{\partial x_1}{\partial x}$$

$$= -\frac{V_0 S(x_1)}{\beta(1 - \beta \varepsilon_1)} \sqrt{\frac{\eta_1}{\eta_2}} \tag{A-17}$$

$$\phi_{z_1} = -\frac{V_0 S(x_1)}{\beta} \sqrt{\frac{\eta_1}{\eta_2}} \frac{\partial x_1}{\partial z}$$

$$= \frac{V_0 S(x_1)}{1 - \beta \varepsilon_1} \sqrt{\frac{\eta_1}{\eta_2}}$$

where the forecone from the receiving point traces directly to x_1 without first passing through or around a body and the area inside the characteristic has a local x maximum at x_1. The z direction in this case is the outward normal from the sending panel at x_1. In the most common case, $x_1 = x$ and $r_1 = r_Q$.

The second part of the x and z derivatives comes from the derivative of the lateral limits of integration. This contribution exists only when $x > x^*$ and the limit is not a characteristic. Differentiating the ω limits of Eq. (A-7),

$$\phi_{x_2} = -\frac{}{\pi} \int \frac{}{} \left[\frac{}{} - \frac{}{} \right]$$

$$\phi_{z_2} = -\frac{}{\pi} \int \frac{}{} \left[\frac{}{} - \frac{}{} \right]$$

Substituting Eqs. (A-15), (A-16) and (A-5), we get

$$\phi_{x_2} = \frac{}{} \int \frac{}{} \left[\frac{}{} \right]$$

$$\phi_{z_2} = -\frac{}{} \int \frac{}{} \left[\frac{}{} \right]$$

except use zero when ω_L or ω_R are on a characteristic.

The third part of the x and z derivatives comes from differentiating the integrand of Eq. (A-8):

$$\phi_{x_3} = \frac{}{} \int \frac{}{} \left[F \frac{}{} \right]$$

$$- \frac{}{} \int \frac{}{} \left[\frac{\partial F}{} \right]$$

$$\phi_{z_3} = -\frac{}{\pi} \int \frac{}{} \left[\frac{}{} \right]$$

$$- \frac{}{} \int \frac{}{} \left[\frac{}{} \right]$$

Combining the contributions from Eqs. (A-17), (A-19 and (A-20), we get for ϕ_X:

$$\phi_x = -\frac{V_0 S(x_1)}{\beta(1-\beta\epsilon)}\sqrt{\frac{n_1}{n_2}}$$

$$+\frac{2V_0}{\pi}\int_0^{x^+}\frac{n_1 S(x_1)(x-x_1)}{\beta^3\left[\frac{(x-x_1)^2}{\beta^2}-(n_2-n_1)^2\right]^{3/2}}\left[F(k_1,\psi)+\frac{8n_1n_2\frac{\partial F(k_1,\psi)}{\partial k_1^2}}{\left(\frac{x-x_1}{\beta}\right)^2-(n_2-n_1)^2}\right]dx_1$$

$$-\frac{V_0}{\pi}\int_{x^+}^{x_2}\frac{S(x_1)(x-x_1)}{\beta^3}\left[\frac{1}{2n_2\sqrt{n_1n_2}}\frac{\partial F(k_2,\omega)}{\partial k_2^2}\right.$$

$$\left.-\frac{2n_1\sin\omega}{\cos\omega\cos\psi\left[\left(\frac{x-x_1}{\beta}\right)^2-(n_2-n_1)^2\right]^{3/2}}\right]dx_1 \qquad (A-21)$$

and for ϕ_Z:

$$\phi_z = \frac{V_0 S(x_1)}{1-\beta\epsilon}\sqrt{\frac{n_1}{n_2}}$$

$$-\frac{2V_0}{\pi}\int_0^{x^+}\frac{n_1 S(x_1)}{\beta^2\left[\frac{(x-x_1)^2}{\beta^2}-(n_2-n_1)^2\right]^{3/2}}\left[(n_2-n_1)F(k_1,\psi)+2n_1\frac{\partial F(k_1,\psi)}{\partial k_1^2}\frac{\frac{(x-x_1)^2}{\beta^2}+n_2^2-n_1^2}{\frac{(x-x_1)^2}{\beta^2}-(n_2-n_1)^2}\right]dx_1$$

$$+\frac{V_0}{\pi}\int_{x^+}^{x_2}\frac{S(x_1)}{\beta}\left[\frac{1}{2n_2}\sqrt{\frac{n_1}{n_2^3}}\left\{F(k_2,\omega)+\frac{\partial F(k_2,\omega)}{\partial k_2^2}\right\}\frac{\frac{(x-x_1)^2}{\beta^2}+n_2^2-n_1^2}{2n_2n_1}\right.$$

$$\left.-\frac{n_1\left\{\frac{(x-x_1)^2}{\beta^2}+n_2^2-n_1^2\right\}\sin\psi}{n_2\left[\frac{(x-x_1)^2}{\beta^2}-(n_2-n_1)^2\right]^{3/2}\cos\omega\cos\psi}\right]dx_1 \qquad (A-22)$$

The ϕ_x and ϕ_z integrands are functions of incomplete elliptic integrals of the first kind and their derivatives with respect to the square of the modulus. The amplitude may be negative, and $F(k, -\psi) = -F(k, \psi)$. The ϕ_y equation (A-10) is much simpler and contains no elliptic integrals.

Several pertinent facts regarding Eqs. (A-10), (A-21) and (A-22) are: (1) the non-integral terms occur whenever the characteristic from the receiving point intersects the sending panel at a right angle without around or passing through any intervening surface and either the sending panel is convex, or the sending panel is concave and the (y,z) projection of the receiving point lies between the panel arc and the center of the arc; (2) the integral terms are actually lateral summations over all of the panels within the bounds of the characteristics and X* may be different for each panel; (3) the terms containing cos ω must be set to zero when the ω limit is a characteristic; (4) the positive z and $\mu = \psi = \omega = 0$ directions are defined by the vector from the (y, z) center of the sending panel arc to the (y, z) projection of the receiving point if the sending panel is convex, and the reverse if the panel is concave; (5) the moduli of the elliptic integrals are defined by

$$k_1 = \frac{\sqrt{4 r_0 r_1}}{\sqrt{(r_0 + r_1)^2 + (z_0 - z_1)^2}}$$

$$k_2 = \frac{1}{k_1}$$

and (6) the amplitudes are related to the real angle μ by

$$\psi = 1/2\ \mu$$

$$\omega = \sin^{-1}(k_1 \sin\psi)$$

A.2 Flat Panel with Linear Lateral Source Strength Variation

Flat panel, as used here, refers only to the lateral shape. The panel may have longitudinal curvature and twist. The positive z direction is the outward normal direction from the sending panel, and will vary with x along the panel. If we define the source strength as

$$S(x_1) = e_0 + e_1 y \qquad (A\text{-}25)$$

where e_0 and e_1 are functions of x_1, the velocity potential is:

$$\phi = -\frac{V_0}{\pi} \int \frac{(e_0 + e_1 y_1)\, dx_1\, dy_1}{\sqrt{(x-x_1)^2 - \beta^2(y-y_1)^2 - \beta^2(z-z_1)^2}} \qquad (A\text{-}26)$$

Carrying out the lateral integration from the left side, y_L, to the right side, y_R, of a panel we get

$$\phi = \frac{V_0}{\pi} \int_{x_L}^{x_R} \left[e_1 \sqrt{\frac{(x-x_1)^2}{\beta^2} - (y-y_L)^2 - (z-z_1)^2} \right.$$

$$\left. - (e_0 + e_1 y_L) \cosh^{-1} \frac{y - y_L}{\sqrt{\frac{(x-x_1)^2}{\beta^2} - (z-z_1)^2}} \right]_{y_L}^{y_R} \frac{dx_1}{\beta^2}$$

Now we will differentiate with respect to x, y and z to obtain the perturbation velocities. Wherever there is a local maximum of x_c or x_1, the derivatives of the limit are as derived in Eq. (A-12) and again $\partial x_1 / \partial y = 0$. At a local maximum of x_c or x, the integrand at y_R minus the integrand at y_L is $-e_0 \pi$, so the derivative of limit terms are

$$\phi_{x_1} = -\frac{V_0 e_0(x_1)}{\beta\sqrt{1-\beta^2 e_1^2}} \qquad (A\text{-}28)$$

$$\phi_{z_1} = \frac{V_0 e_0(x_1)}{\sqrt{1-\beta^2 e_1^2}}$$

When y_R and y_L are not characteristics, they are not functions of x, y, or z so there is no derivative of lateral limit contribution.. When y_R or

y_L are on a characteristic, the integrand is infinite, so in order to take only the finite part we again neglect the derivative of lateral limit term.

Adding the x derivative of the integrand to the derivative of limit term in Eq. (A-28),

$$\phi_x = -\frac{V_\infty \ell_c(x_1)}{\beta(1-\beta\epsilon_1)} \qquad (A\text{-}29)$$

$$-\frac{V_\infty}{\pi}\int_0^{x_c - \frac{(y-y_1)\ell_c(x_c+x,y)}{\beta}} \frac{-\ell_1}{\sqrt{\left(\frac{x-x_1}{\beta}\right)^2-(z-z_1)^2-(y-y_1)^2-(z-z_1)^2}} \frac{\ell_x(x-x_1)}{\beta^3}$$

and similarly for the z derivative,

$$\phi_z = \frac{V_\infty \ell_c(x_1)}{1-\beta\epsilon_1} \qquad (A\text{-}30)$$

$$+\frac{V_\infty}{\pi}\int_0^{x_c - \frac{(y-y_1)\ell_c(x_c+x,y)}{\beta}} \frac{-\ell_1}{\sqrt{\left(\frac{x-x_1}{\beta}\right)^2-(z-z_1)^2-(y-y_1)^2-(z-z_1)^2}} \frac{(z-z_1)\ell_x}{\beta}$$

Note that the ϕ_z integrand is identical to the ϕ_x integrand, except the sign is changed and $(x-x_1)/\beta^3$ is replaced by $(z-z_1)/\beta$.

The only contribution to ϕ_y is the derivative of the integrand:

$$\phi_y = \frac{V_\infty}{\pi}\int_0^{x_c} \left[-\ell_1 \left/ \sqrt{\left(\frac{x-x_1}{\beta}\right)^2-(z-z_1)^2}\right.\right]\frac{y-y_1}{\beta^2}$$

$$+\frac{\ell_c + \ell_1}{\sqrt{\left(\frac{x-x_1}{\beta}\right)^2-(y-y_1)^2-(z-z_1)^2}}\ell_x \frac{dx}{\beta}$$

Several pertinent facts regarding Eqs. (A-29), (A-30) and (A-31) are : (1) the non-integral terms occur whenever the characteristic from the receiving point intersects the sending panel at a right angle without wrapping around or passing through any intervening surface; (2) the integral terms are actually lateral summations over all of the panels within the bounds of the characteristics; (3) the terms containing

$$\frac{\sqrt{(x-x_1)^2-(y-y_1)^2-(z-z_1)^2}}{\beta}$$

must be set to zero when the y limit is a characteristic; and (4) the positive z direction is defined by the outward normal from the sending panel.

APPENDIX B

COMPUTER USER'S MANUAL FOR IMPROVED WAVE DRAG PREDICTION METHOD USING MODIFIED LINEAR THEORY

TABLE OF CONTENTS

1.0 INTRODUCTION

This report describes Vought's Improved Wave Drag "Analysis Routine", and an interactive computer "graphics routine" to view and edit the input data deck to be used with the analysis routine. The analysis routine computes local velocities and pressures on the surface of the configuration and integrates the pressures to obtain lift, drag and pitching moment. At the present stage of development, the analysis routine can handle a single body with inlet or exhaust surfaces approximately perpendicular to the free stream, and one pair of wing panels in a horizontal plane. The wing data can not be input to or displayed by the graphics routine. The data deck describes the external skin contour of an aircraft fuselage which can have longitudinal steps, and may have a blunt nose and discontinuous body slopes or curvature. The input data consists of three dimensional point definitions, together with sufficient information to divide the points into rows and body sections, to identify lines of slope or curvature discontinuity, and to indicate any "covered" areas where no boundary conditions are applied and the source strength is zero. No surface slope information is input by the user.

The program uses a three dimensional parametric cubic space spline to define slopes along curves connecting input points both laterally and longitudinally. These space curves then are used to define "Coon's patches" (parametric cubic surface patches). The resulting surface definition is guaranteed to be continuous in position as well as first and second derivative except along lines that the user has identified as slope or curvature discontinuities. The configuration is assumed to be left-right symmetric.

Local velocities and pressures are calculated to two to six points on each panel, and the source strength varies linearly in both directions on the panel. The source strength is continuous across panel boundaries, unless the surface slope is discontinuous. Because of these techniques and the curved panel definitions, the panels can be quite large in regions where the velocities and source stengths are not expected to vary rapidly. For example, in a region where the configuration is nearly axisymmetric, the panels could span thirty degrees or more laterally. In general, the input deck should contain a much smaller number of points than would be required for an area rule input deck describing the same configuration. A permanent restriction on

the longitudinal location of points within a row is that the slope (after rotation) of the fore and aft panel boundaries must be less than $\sqrt{M_T^2 - 1} / \sqrt{1 + \epsilon^2}$ relative to the Y-Z plane, where M_T is the larger of true local Mach number and 1.1, and ϵ is the panel surface slope. The program will automatically rotate the input geometry to an input value of angle of attack.

The graphics routine has been implemented on a CDC 6600, CDC Cyber 175, and a PRIME mini-computer with a Tektronix 4014 using the Plot 10 software package. However, the program was written to be easily transportable to any type of graphics scope.

2.0 GEOMETRY CONCEPT

The fuselage external surface is defined by a set of three dimensional point definitions. A right-handed X-Y-Z coordinate system is used: positive X is aft, positive Y is the right side, and positive Z is up. Points are input in rows, and the resulting set is connected both laterally and longitudinally. While the analysis routine only requires lateral point connectivity, the splining technique used to determine body slopes requires the connectivity in two directions. Thus, each row within a section must have the same number of points. Points are ordered from bottom to top, and the rows are ordered from front to rear. Lateral symmetry is assumed and only the positive Y half of the fuselage is defined.

The wing geometry is planar, and may be defined by airfoil ordinates, standard airfoil definitions or streamwise slope inputs.

3.0 INPUT FORMAT

3.1 INPUT DATA DECK, EXCLUDING WING DATA

The data deck, except for the wing data if used, consists of only five types of cards: title cards, point definition cards, an END card, an S_{ref} card, and a Mach number card. A case begins with two title cards. The first 40 columns of both cards are displayed on the scope. Following the title cards, each card contains a single point definition, with five free format data fields in the first 40 columns. Columns 41-80 can be used for

comments. Data fields are separated by blanks or commas and may be numeric or alphabetic. A field is interpreted as numeric if the first character is numeric (0-9, plus, minus, or decimal) and is alphabetic if the first character is A-Z. A decimal is assumed to the right of a numeric field if none is present within the field.

The five data fields are the X, Y, and Z values for the point and two point type fields. The coordinate fields may be numeric or may be defined by the letters "X", "Y" and "Z", to indicate to use the previously defined value. The point type serves three purposes. It indicates the division of points into rows and sections, indicates slope or curvature discontinuities, and indicates edges of covered panels. Point type is an alphabetic field. The first character indicates whether the point initiates a section ("S"), initiates a row ("R"), is a corner point ("C"), is a curvature discontinuity ("D"), is a covered area ("V"), or is a normal point (anything else). If the first character is an "S", "R" or "C", the second and third characters can indicate the direction of a slope discontinuity. An "X" indicates a longitudinal discontinuity and a "Y" indicates a lateral discontinuity. Any other characters except "D" are ignored. For example, "CY" indicates a point at which the slope is discontinuous in the lateral direction, and "RX" indicates the beginning of a row at which the longitudinal slope changes. "C_" is interpreted as "CY". If a point is both a corner point (slope discontinuity) and a curvature discontinuity, the slope discontinuity must be indicated first (e.g., CXDY or RYDX). The initial point of a data set is automatically assigned as "S" by the program. If less than four fields are supplied, the previous values are assumed for the missing X, Y or Z fields and "normal point" for the point type. Point definition input is terminated by the letters "END" in the first data field of a card. When wing data are input, they are inserted after the body data are completed and before the END card (see Sction 3.2 below). Next is the S_{ref} card with reference area and reference chord and geometry rotation angle (degrees) in three data fields (free format). There must be at least two non-zero values on this card. The last input card contains analysis Mach numbers in free format, with a maximum of 19 values. The minimum Mach number allowed is 1.1 The second "Mach number" may be used as an indicator - e.g., 0 for only wing-alone calculations, -n to restart at row n.

The covered area indicator ("V") appears in the fifth data field unless the point type is noraml (blank, not a row or section initiator). If the fourth field would otherwise be blank, the V goes in the fourth data field. Any additional characters in the V field are ignored. In any lateral row of points, there must be either zero or two V indicators. The V indicator has no effect on the surface splining. When the V indicators are matched by V's on an adjacent row at the longitudinally connecting pairs of points, the analysis routine is triggered to bypass satisfying the no-flow-through boundary condition on the intervening panel or panels and to set the source strength on those panels to zero.

When the fuselage cross-section is a circle and seven evenly spaced lateral points will match up with adjacent rows in the section, a simple radius and Z location can be input instead of the seven X, Y, Z values, (I.e., one card can define a complete row.) In this case, the five data fields are X, radius, "AX", point type and Z center. The "AX" in the third field may have additional characters after the AX, which will be ignored. The point type can only be S, SUX, R, RX or RUX. The Z center shifts the center of the section vertically, if desired. The program computes the X, Y and Z of the seven evenly spaced (30 degrees) lateral points.

3.2 WING INPUT DATA DECK

The additional input data for the wing is inserted after the body data is completed and before the END card. The wing data begins with WING in the first free format data field of a card. At present, the wing data cannot be included in the input to the graphics routine.

When wing data are input, the rotation angle of the S_{ref} card must be zero, and there must be only one real ($\geq$ 1.1) Mach number. If only a wing-alone calculation is desired, input two Mach numbers with the second one equal to zero. The reference area input to or calculated by the wing routine will override the reference area on the S_{ref} card described bove. Also note that the drag values printed with the body calculations do not include the wing drag and vice versa.

The wing surface is defined by airfoil sections. The input can consist of an area rule deck or surface slopes which will be curve-fitted. The wing

planform may be trapezoidal or it may have one leading edge break (two sweep angles) and up to three trailing edge breaks (four trailing edge sweep angles). The wing geometry is flattened into a Z=constant plane through the Z value of the root chord. There is an upper limit of six spanwise curve fit intervals, which means that with an area rule input, a maximum of 7 span stations can be input unless a discontinuity flag or duplicate span station locations (Y, Z) are used.

The wing inputs are described in the following figures and definitions.

WING DATA INPUTS

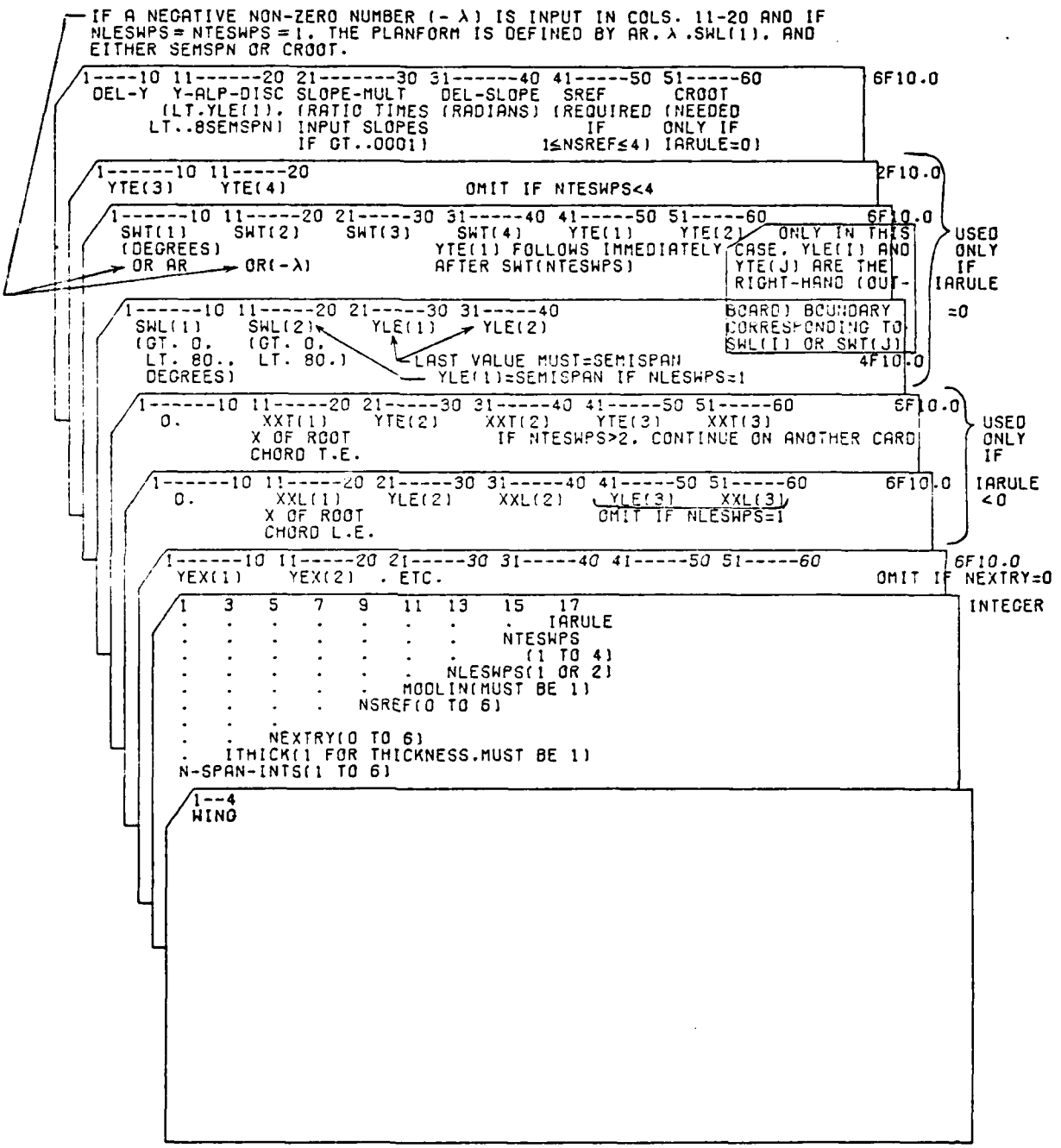

NOTE N'S ARE NEEDED ONLY IF AIRFOIL HAS CORNERS AND FNORD>5.
IF N'S ARE USED THE CHORDWISE CURVEFIT OF THE AIRFOIL
SLOPES WILL BE DISCONTINUOUS AT X/C_N'S I.E., THE VALUES
OF X/C_N DEFINE THE CHORDWISE CURVEFIT BOUNDARIES.

NOTE PROGRAM SHOVES LEFT AND RIGHT WING PANELS TOGETHER
IF THIS IS NOT DESIRED BUT Y(1)>0. 2 ADDITIONAL AIRFOILS
AT Y=0 AND Y=Y(1) WITH ORDINATES=0 MUST BE ADDED.
ALSO PROGRAM FLATTENS THE WING($\Delta Y = \sqrt{\Delta Y^2_{input} + Z^2_{input}}$)

1-----10 11----20 21----30 31----40 41--50 51--60 61--70 71--80 8F10.0
Z/C, Z/C$_2$ Z/C$_3$,ETC.
SEMI-THICKNESSES OF THIS AIRFOIL. IN EITHER PERCENT CHORD OR FRACTION OF CHORD
OMIT IF STANDARD AIRFOIL OPTION (AFID) IS USED
Z/C'S CONTINUE ON SUBSEQUENT CARDS IF FNORD>8

REPEAT NAF TIMES, 2≤NAF, NAF≤12, BUT 6 OR LESS CURVE-FIT INTER-VALS

1-----10 11----20 21----30 31----40 41----50 51----60 61---70 73 76 78
X_{LE} Y Z CHORD AFID XTMAX DISC FLG N, N_2 N_3
AFID 55A0044.FOR EXAMPLE OR 63A.OR 64A. OR BIC
EITHER % OR FRACTION
OR T/C
7F10.0. 3I3

1-----10 11----20 21----30 31----40 41--50 51--60 61--70 71--80 8F10.0
X/C, X/C$_2$ X/C$_3$,ETC.
VALUES OF X/C CAN BE EXPRESSED IN EITHER PERCENT CHORD OR FRACTION OF CHORD. ONE SET OF VALUES APPLIES TO ALL AIRFOILS
OMIT IF FNORD < 3.
X/C'S CONTINUE ON SUBSEQUENT CARDS IF FNORD>8

1------10 11-----20 21-----30 31-----40 4F10.0
XORIG YORIG ZORIG FNORD
IF FNORD < 3., THE X/C CARD IS OMITTED. THE PROGRAM SETS FNORD = 13. AND USES EVERY 10% CHORD.PLUS 5% AND 15%

1-3 11-----20 A3,7X,A10
I03 NAME
6 (ADDED TO END OF TITLE)
OR 7

NOTE X_{LE}.Y.Z. AND CHORD VALUES MUST BE SUCH THAT THE RESULTING (FLATTENED) WING HAS NO MORE THAN 2 L.E. AND 4 T.E. SWEEP ANGLES.
TOLERANCE IS $\Delta(\tan\Lambda_{LE}) < .01745$, $\Delta(\tan\Lambda_{TE}) < .01745$

AREA RULE INPUT(S4007)
DATA ON THIS PAGE IS USED ONLY IF IARULE=1

NOTE N'S ARE NEEDED ONLY IF AIRFOIL HAS CORNERS AND NWAFOR>5.
IF N'S ARE USED THE CHORDWISE CURVEFIT OF THE AIRFOIL
SLOPES WILL BE DISCONTINUOUS AT XAF_N ; I.E., THE VALUES
OF XAF_N DEFINE THE CHORDWISE CURVEFIT BOUNDARIES.

NOTE PROGRAM SHOVES LEFT AND RIGHT WING PANELS TOGETHER
IF THIS IS NOT DESIRED BUT Y(1)>0. 2 ADDITIONAL AIRFOILS
AT Y=0 AND Y=Y(1) WITH ORDINATES=0 MUST BE ADDED.
ALSO PROGRAM FLATTENS THE WING($\Delta Y = \sqrt{\Delta Y^2_{true} + \Delta Z^2_{true}}$)

1----7 8---14 15--21 22--28 29--35 36--42 43--49 50--56 57--63 64--70	10F7.0
WAFORD, WAFORD, WAFORD, WAFORD, WAFORD, WAFORD, WAFORD, WAFORD, WAFORD, WAFORD,	REPEAT NWAF TIMES
SEMI-THICKNESSES OF THIS AIRFOIL	
OMIT IF STANDARD AIRFOIL OPTION (AFID) IS USED	
WAFORD'S CONTINUE ON SUBSEQUENT CARDS IF NWAFOR > 10	

1---7 8---14 15--21 22--28 41----50 51----60 61----70 73 76 79	4F7.0.
X_{LE} Y Z CHORD AFID OR T/C XTMAX DISC.FLG N_1 N_2 N_3	12X.
	3F10.0.
	3I3
REPEAT THIS CARD NWAF TIMES	

1---7 8---14 15--21 22--28 29--35 36--42 43--49 50--56 57--63 64--70	10F7.0
XAF_1 XAF_2 XAF_3 XAF_4 XAF_5 XAF_6 XAF_7 XAF_8 XAF_9 XAF_{10}	
OMIT IF NWAFOR < 3	
XAF'S CONTINUE ON SUBSEQUENT CARDS IF NWAFOR > 10	

INTEGER

16 20
NWAF NWAFOR
(2 TO 12) (3 TO 25)

← BUT FOR NWAF > 7 TO BE ALLOWABLE,
EITHER DISC. FLAG OR TWO AIRFOIL DEFS. AT THE
SAME Y,Z MUST BE USED SO THAT 6 OR LESS
SPANWISE CURVEFIT INTERVALS RESULT.

NOTE X_{LE}, Y, Z, AND CHORD VALUES MUST BE SUCH THAT THE
RESULTING (FLATTENED) WING HAS NO MORE THAN 2 L.E.
AND 4 T.E. SWEEP ANGLES.
TOLERANCE IS $\Delta(\tan\Lambda_{LE}) < .01745$, $\Delta(\tan\Lambda_{TE}) < .01745$

AREA RULE INPUT(TMX-947)
DATA ON THIS PAGE IS USED ONLY IF IARULE=2

IF JCONIC > 0, α IS INTERPOLATED AS A FUNCTION OF $\frac{X-(E_{n-1}+F_{n-1}*Y)}{(E_n+F_n*Y)-(E_{n-1}+F_{n-1}*Y)}$ INSTEAD OF X/C

```
1------10 11-----20 21-----30 31-----40 41-----50 51-----60                6F10.0
(X/C)3      α3      (X/C)4      α4      (X/C)5      α5
                                                    OMIT IF NSPALP=1 OR 2
THIS CARD USED ONLY IF NPN>2(ADDITIONAL CARDS NOT SHOWN ARE USED IF NPN>5)

1------10 11-----20 21-----30 31-----40 41-----50 51-----60                6F10.0
  Y3      ALP-MULT    (X/C)1      α1      (X/C)2      α2
                                                    OMIT IF NSPALP=1 OR 2
NOTE: DO NOT PUT AN INTEGER IN COLUMN 1(COL.1 IS PART OF THE Y3 FIELD)

1------10 11-----20 21-----30 31-----40 41-----50 51-----60                6F10.0
(X/C)3      α3      (X/C)4      α4      (X/C)5      α5
                                                    OMIT IF NSPALP=1
THIS CARD USED ONLY IF NPN>2(ADDITIONAL CARDS NOT SHOWN ARE USED IF NPN>5)

1------10 11-----20 21-----30 31-----40 41-----50 51-----60                6F10.0
  Y2      ALP-MULT    (X/C)1      α1      (X/C)2      α2
                                                    OMIT IF NSPALP=1
NOTE: DO NOT PUT AN INTEGER IN COLUMN 1(COL.1 IS PART OF THE Y2 FIELD)

1------10 11-----20 21-----30 31-----40 41-----50 51-----60                6F10.0
(X/C)3      α3      (X/C)4      α4      (X/C)5      α5

THIS CARD USED ONLY IF NPN>2(ADDITIONAL CARDS NOT SHOWN ARE USED IF NPN>5)

1 2----10 11-----20 21-----30 31-----40 41-----50 51-----60 61----70   :1,F9.0,
. Y1      ALP-MULT    (X/C)1      α1      (X/C)2      α2      JCONIC,  5F10.0,I10
NPN                                                         ALTERNATE
(1 TO 9)          NOTE α IS IN RADIANS                      CURVEFIT OPTION
                                                          REPEAT NXINT TIMES

1 3 4---10 11----20 21-----30 31-----40 41-----50 51-----60 61-----70  11,12,7X,
. . BLANK    E1         F1         E2         F2         E3         F3   6F10.0
. NSPALP(NORMALLY 1 TO 3.IF LEFT BLANK IS SET TO 3. BUT IF A NEGATIVE
. VALUE IS INPUT, THEN IC CURVE-FIT COEFFICIENTS WILL BE READ IN 6F10.0
. FORMAT INSTEAD OF X/C,α DATA ABOVE)
NXINT              IF "BLANK" IS NOT BLANK.THE CURVEFIT BOUNDARIES ARE
(1 TO 4)           DEFINED AS X/C'S
                                                  REPEAT N-SPAN-INTS TIMES

1------10 11-----20 21-----30 31-----40 41-----50 51-----60                6F10.0
AY(1)      AY(2)      AY(3)      AY(4)      AY(5)      AY(6)
(=0.)

                    AY(I) IS THE LEFT-HAND OR INBOARD BOUNDARY
                    OF THE I TH CURVE-FIT INTERVAL; AN * IN THE
                    FIRST COLUMN OF AN AY FIELD (11,21,ETC.)
                    INDICATES A SPANWISE SLOPE DISCONTINUITY-
                    RESULTS IN AN EXTRA Y AND SPECIAL INTEGRATION
                    TREATMENT

          THIS CARD OMITTED IF N-SPAN-INTS=1

1------10 11-----20 21-----30                                              3F10.0
 RUTX       RUTY       RUTZ

     X,Y,Z COORDINATES OF ROOT CHORD LEADING EDGE


ALL DATA ON THIS PAGE OMITTED IF IARULE > 0
```

SYMBOL DEFINITIONS

Notation

Symbol	Definition	Units
N-SPAN-INTS	Number of spanwise curve-fit intervals	None
ITHICK	Thickness option; ITHICK = 0 for camber, twist and angle of attack effects, ITHICK = 1 for thickness effects	None
NEXTRY	Number of extra span stations (in addition to those determined by multiples of DEL-Y) for aero calculations	None
NSREF	Reference area option; NSREF = 0 total plan area will be used; NSREF = 1 input value of SREF will be used in same units as planform dimensions; NSREF = 2 input value of SREF will be used assuming SREF is in ft^2 and dimensions are in inches; NSREF = 3 input value of SREF used as a ratio, i.e., reference area = SREF × plan area; NSREF = 4 reference area = plan area plus an extension inboard of SREF inches (or whatever units are being used), this is useful for thickness drag cases where exposed panels have been skewed together for reflection plane effect; NSREF = 5 reference area defined by outermost wing panel extended in to the centerline; NSREF = 6 reference area defined by innermost wing panel extended out to the tip station.	None
MODLIN	Nonlinearity option; pressure coefficients calculated from the exact equation using calculated streamwise pertubation velocity and assumed spanwise pertubation velocity. In addition, when ITHICK=1, local β (forecone shape) is modified to account for local perturbed velocity and the flow tangency condition uses local velocity rather than free-stream velocity in denominator (available only for thickness effects, ITHICK = 1). MODLIN = 1 gives nonlinear solution; MODLIN = 2 gives nonlinear solution plus linearized solution with modified tangency condition only; MODLIN = 3 gives only a printout of the modified slopes in addition to the usual linearized solution	None

Symbol	Definition	Units
NLESWPS	Number of sweep angles used to define leading edge of planform	None
NTESWPS	Number of sweep angles used to define trailing edge of planform	None
IARULE	Geometry and slope input option. If IARULE > 0 (allowed only if ITHICK > 0, JSYM = 0, JTWIST ≤ 0, and KONIC = 0), the wing definition portion of an area rule input deck provides both the wing geometry and airfoil (slope) inputs. If IARULE = 1, Vought format is used and if IARULE = 2, NASA (TM X-947) format is used. If IARULE ≤ 0, slope inputs are required. If IARULE < 0, geometry is defined by (Y, X) coordinates. If IARULE = 0, geometry is defined by leading and trailing edge sweep angles	None
YEX(I)	Extra span stations for aero calculations	*

Symbol	Definition	Units
XXL(I)	X coordinate of the leading edge at YLE (I)	*
YLE(I)	Span station defining leading edge break point.	*
XXT(J)	X coordinate of the trailing edge at YTE(J)	*
YTE(J)	Span station defining trailing edge break point	*
SWL (I)	Leading edge sweep-back angle, SWL(n) is the sweep inboard of YLE(n).	Degrees
SWT(J)	Sweep defining trailing edge of planform SWT(n) is sweep inboard of YTE(n).	Degrees
DEL-Y	Increment in y between calculated span station; if left blank or made less than 0.1 semi-span, it will be set equal to 0.1 semi-span for lift cases and 0.2 semi-span for thickness cases.	*
Y-ALT-DISC	Span station at which the constant (fuselage) α interval ends; must be exactly equal to AY(2) if used.	*
SLOPE-MULTIPLIER	Factor by which all input slopes, except conical camber (α_c) will be multiplied: if absolute value is < .0001, program sets to 1.0. Not used if α = CyTWIST	None
DEL-SLOPE	Constant, to be added to input α distribution.	Radians
SREF	See XSREF	-
CROOT	Root Chord.	*

Symbol	Definition	Units
AY	Spanwise curve fit boundaries; value is equal to the y value of the left boundary of the respective span interval.	*
C	Twist case only (JTWIST ≥ 0 and N-SPAN-INTS = 1), $\alpha = Cy^{JTWIST}$.	Radians/ (*) JTWIST
NXINT	Number of chordwise curve fit intervals in a given spanwise interval	None
NSTALP	Number of span stations for α inputs	None
E1, F1	Coefficients of boundary between the first and second chordwise intervals where X = E1 + F1 (y)	*
E2, F2	Coefficients of boundary between the second and third chordwise intervals where X = E2 + F2 (y)	*
E3, F3	Coefficients of boundary between the third and fourth chordwise intervals where X = E3 + F3 (y)	*
NPN	Number of input pairs of X/C, α per span station for the particular curve-fit interval being considered	None
Y1, Y2, Y3	The three span stations at which α data is given for the particular curve-fit interval being considered	*
ALP-MULT	Factor by which input α's for this Y and this chordwise interval only will be multiplied. Not used if input value = 0	None
X/C	Fraction of local chord	None
α	Local angle of attack (for ITHICK = 1, $\alpha = -d(t/2)/dX$).	Radians
JCONIC	Curvefit option; if 70, slopes will be fitted and interpolated spanwise along constant fractions of curve-fit panel chord instead of wing chord. This option is chosen separately for each curve-fit interval.	

When an option indicator is 0, the option is not used, when it is 1, the option is used.

*Indicates that the length dimensions must merely be consistent.

4.0 INTERACTIVE PROGRAM CONTROL (GRAPHICS ROUTINE)

4.1 COMMAND SUMMARY

For reasons of initial program portability, all program interaction is handled through the keyboard. All commands are initiated by typing at least the first two characters of the command name. The routine will respond with a prompter describing the additional information (if any) required to complete the command. Commands fall into four categories:

- Display options
- Editing options
- Editing aids
- Output options

The display options give the user control over the appearance of the graphical display. Options are available to view the model from any angle, to change the scale and view center of the display, to clip the display to a three dimensional view box, to display either or both sides of the model, and to clear the screen and re-display the model.

The editing options allow the user to change the title, move one or more points, change the corner codes, or to reject the effect of the previous change.

Editing aids allow the user to mark a number of points on the display with their point numbers, or to display the coordinates and corner codes for one or more points.

Output options include the ability to print or punch the current data set, or to plot the display. The "plot" option currently just writes a vector file which can be processed by an external routine to route the information to an appropriate plotting device. Two examples of the scope display are shown in Figures 1 and 2.

4.2 DISPLAY COMMANDS

For display purposes, the complete model definition is stored as a single vector list, in model coordinates. When the program calls for the display of the model, each vector is processed by the following transformations:

1) Translate with respect to a view center
2) Rotate through yaw, pitch and roll angles
3) Scale to a specified unit sphere
4) Clip to a specified three dimensional viewport

The remaining visible portion of each vector (if any) is displayed with the X coordinate mapping onto the horizontal screen dimension and the Z coordinate mapping onto the screen vertical dimension.

The display options allow the user to specify the parameters used in the viewing transformations as well as to control re-displaying the model and to select one or both sides of the model for display.

Since the user may wish to change several of the display parameters before re-displaying the picture, an optional display suppression flag may be input following the last mentioned parameter. When any non-blank value is supplied for this flag, the picture will not be re-displayed until a further command specifically requires it.

4.2.1 Translate

The program responds with "ENTER VIEW CENTER X, Y, Z". The user should type the model coordinates of the point that will be translated to the center of the screen.

4.2.2 Rotate

The program responds with "ENTER YAW, PITCH, ROLL". The user should type the values in degrees. The (0, 0, 0) orientation is the left profile. Positive yaw is nose left. Positive pitch is nose up. Positive roll is right side up.

A convenient way to visualize a desired rotation is to image that the viewer is initially located to the left side. First move around toward the nose by the desired yaw angle. Then move the imaginary viewpoint through a desired elevation angle. The pitch angle will be the negative of the elevation angle and roll will be zero. The model can be viewed from any angle with only two angles specified. Three rotation angles are necessary only to control the orientation of the resulting view.

4.2.3 Scale

The program responds with "ENTER VIEWING RADIUS". The user enters a radius, in model coordinates, that will be scaled to fit within a 12-inch viewing area.

4.2.4 Clip

The program responds with "ENTER XMIN, YMIN, ZMIN, XMAX, YMAX, ZMAX". The values are in display coordinates (screen inches). (0, 0, 0) is the screen center. The following may aid in specifying the values.

XMIN - Left side
YMIN - "Near" side. Negative Y is toward the viewer
ZMIN - Bottom
XMAx - Right side
YMAX - "Back" side. Positive Y is behind the screen
ZMAX - top

4.2.5 Side

This controls whether the program displays the left side (-Y), the right side (+Y), or both sides of the model. The program responds "LEFT, RIGHT OR BOTH".

4.2.6 Paint

This causes the program to clear the screen and re-display the picture. This may be necessary because of an accumulation of command or output data on a Tektronix scope.

4.3 EDITING AIDS

The commands are available to aid the user in identifying and locating points on the display.

4.3.1 Mark

This command causes the program to show the point number of one or more points on the display at the point location. This enables the user to identify points in the configuration. The program responds with "ENTER POINT RANGE". The user types in the first and last numbers to be marked. Once a range of points has been marked, the command stays in effect through changes of display until changed. To turn off the point marking, enter null print range (0, 0 or only a space before the end-of-line).

4.3.2 Locate

The program responds "ENTER POINT RANGE". After the user types in the first and last point of interest, the program will display the existing X, Y and Z coordinates and the corner code for the specified points.

4.4 EDITING COMMANDS

Four commands are available that actually change the data set. These allow the user to move points, change the corner codes, reject a previous change, or change the title.

4.4.1 Move Points

The program responds "ENTER POINT RANGE, X, Y Z". The user enters the first and last point to be moved (which may coincide) and the new point coordinates for the first point of the range. All the points will then be moved by the same increment as the first point. This allows an entire row or group of rows to be moved as easily as a single point.

4.4.2 Change Corners

The program responds "ENTER POINT RANGE AND NEW CORNER CODE". The user enters the first and last point of interest and the new ten character point type, which can include the regular point type field and/or the "V" indicator for covered panels. Notice that the routine will not redefine rows or sections with this command, only the slope discontinuity indicators are changed.

4.4.3 Reject

This command retracts the effects of the previous MOVE or CHANGE command. No additional parameters are entered.

4.4.4 Title

The routine responds "TYPE IN FIRST LINE OF NEW TITLE" and then "TYPE IN SECOND LINE OF NEW TITLE". Forty characters may be entered in each line.

4.5 OUTPUT COMMANDS

Three output options are available to allow the user to print or punch the current data set, or to write a plot file.

4.5.1 Print

No other parameters are entered. The printed output represents the current title, point and corner codes.

4.5.2 Punch

No other parameters are entered. The punch deck may be used for direct input either to the graphics/editing routine or to the analysis routine later.

4.5.3 Plot

No other parameters are entered. The routine writes a binary file consisting of the current vector set and view transformation parameters for use by an external batch routine to direct the required plot data to the appropriate plotting equipment. If the vector set has not changed since the previous plot was requested, only the new view parameters are written.

5.0 SAMPLE CASE

Printout for a sample case is shown in Figure 3. Included in the printout is a side by side literal and interpreted print back of the fuselage input data. If a wing is input, the print back is the interpreted type only. Next is the panel geometry data resulting from the three dimensional splining. Finally, the computed local pressures and velocities and the integrated forces are printed.

6.0 SUGGESTIONS FOR INPUT PREPARATION

The most important recommendation is to always use the graphics routine to check and edit the body geometry. This step nearly always uncovers one or more errors in the input data or areas where the curve fit is not quite what was desired.

In general, one should use the minimum number of points which adequately describe the geometry. The only exception is in areas where it is apparent that flow conditions will be varying rapidly due to asymmetry or local slope variations. In areas where flow conditions are nearly constant, a panel can span 30, 45, or even 90 degrees laterally. The panels should not span more than 90 degrees because that could cause inaccuracy in the characteristic tracing.

The body points are input from bottom to top, starting with the front row. Although the input points are sequenced from bottom to top, the panels are numbered from top to bottom and the results are printed in top to bottom order. Each lateral spline fit extends from the bottom point to the first lateral corner (CY) or the top point, and the next one to the next CY or the

top point, whichever occurs first. Each longitudinal line is splined from the first row in the section to the next longitudinal corner (CX or RX) or to the last row in the section, etc. A curvature discontinuity (DX or DY) does not interrupt the fit; it keeps the slope continuous but substitutes a constant curvature condition in an adjacent segment instead of the equal curvature condition across the point. Within each spline fit of more than two points there must be at least one point at which the curvature is continuous.

The discontinuous curvature (DX or DY) option should be used when one class of curve joins another with the slope continuous. An example is a tangent ogive cylinder body shape. Curvature reversals also can occur at locations where it is necessary to keep the slope continuous.

The covered panel (V) option should be used in most cases at the wing-body intersection, particularly if a portion of the wing stub is defined as part of the body, or if lateral corners with $\Delta > 60^{o}$ are adjacent to the covered panel.

A new section is required to change the number of input points per row or to introduce an inlet-type step. At each new section, the spline fit starts anew, and the slopes and ordinates may be different from those at the end of the previous section.

Normally, the slope of the lateral spline fit is $\pm 90^{o}$ at the first and last points in a row. If this is not desired, these points must have a CY point type. Also, the first and last points in each lateral row must lie in the plane of symmetry ($Y < 10^{-6}$x body length). All longitudinal lines defining lateral boundaries of panels must have positive length ($\Delta X > 2 \times 10^{-6}$x body length).

The fore and aft panel boundaries (lateral input rows) have a maximum slope limitation because of the marching scheme used to solve the non-linear equations. The marching scheme requires that succeeding rows not have any effect on the current row. Thus, the characteristics from the back of a row must not trace out of the back of the row. This means that the lateral slope must always be less than $\sqrt{M_t^2 - 1}/\sqrt{1 + \varepsilon^2}$ where M_t is the true local Mach number with a minimum value of 1.1 and ε is the streamwise surface slope. To meet this requirement, all lateral lines should have a slope less than $0.458/\sqrt{1 + \varepsilon^2}$.

When wing data are input, the airfoils can be defined by either of two formats of area rule type input (airfoil ordinates) or by streamwise surface slope input. When surface slope input is used, care must be taken with the sign of the slope. The input is -1//2 dt/dx, so the sign is negative when the thickness is increasing, and positive when the thickness is decreasing.

A restart capability is available to prevent having to duplicate long computations in cases such as encountering the CP time limit, a program bomb, or to evaluate effects of goemetry changes near the aft end of the body. To use this capability, the file TAPE8 must be saved from the initial calculation. Then the calculations can be restarted at the beginning of any row for which all preceding row calculations were completed. E.g., if the initial calculation was completed through row 6, the case can be restarted at any row from 2 through 7. The Mach number must be the same and the geometry through the preceeding row must be unchanged. The program is signaled to use the restart capability by reading the input Mach numbers and finding the second "Mach number" is ≤ -2. The calculation starts at the 'n'th row if the second "Mach number" is (-n). The old TAPE8 file must be attached to the job with the local file name of TAPE8.

7.0 ARRAY LIMITS

a) NPANL $\leq$ 200, where NPANL = actual number of panels + 1 extra (dummy) per row.

b) NROWS $\leq$ 20, where NROWS = numbers of rows of panels (is less than number of input stations by the number of sections).

c) NPL $\leq$ 19, where NPL is the number of actual panels in any row.

d) NYDISC $\leq$ 33-NPL, where NYDISC is the number of Y, or lateral, discontinuities in the row.

e) MLDSC $\leq$ 80, where MLDSC is the total number of Y (lateral) slope discontinuities.

f) NSECS $\leq$ 6, where NSECS is the number of sections.

g) Total number of input points $\leq$ 400.

8.0 OUTPUT DATA FROM ANALYSIS ROUTINE

The output data consists of the following categories in order:

a. Date and time of run
b. Title cards
c. Body geometry input - literal and interpreted, side by side
d. Wing input data-interpreted-if used.
e. Reference area card, Mach numbers - interpreted
f. Summary of sections, rows, points
g. Wing-alone results - if applicable
h. Panel geoemetry
i. Body results
j. Results for wing with effect of body - if applicable

Only items (g) through (j) above will be discussed, because (a) through (f) are self-explanatory.

The wing alone results include chordwise data at each span station and the integrated drag coefficient of the wing based on the specified reference area. The span stations (y's) are relative to the y of the root chord, RUTY. At every 5% of the local chord, values of upper surface ordinate (Z/C) as a fraction of local chord, local slope (ALP= -dz/dx) and pressure coefficient (CPU) are printed. The CDC value is the local section drag coefficient times the local chord, divided by the average chord of the exposed wing.

The panel geometry print gives geometric data on each panel at the four corners and at the average x on each side of the panel. The RDD is a curvature measure; i.e., the second derivative of radius with respect to X. The ordinates X, Y and Z, the derivatives YD (dy/dx) and ZD (dz/dx), the streamwise SLOPE and the outward surface normal THETA are printed at each point from the parametric cubic surface patch definitons. The analysis routine uses a circular arc approximation at each X to the surface patch defined shape. The 1/RADIUS and ARC-THETA are the reciprocal of the circular arc radius and the θ, respectively, associated with the circular arc approximation. Theta is the direction of the projection into an X = constant plane of the local surface outward normal, and θ = 0 is parallel to the positive y axis.

The body results print the calculated pressures and flow conditions at each control point. Control point calculations are made at the beginning (front) of the first row and for other rows when required due to discontinuities. Control point calculations are always made at the middle and back of each row. X, Y and Z are the ordinates of the control point. Control points are located 20 percent of the panel width away from the side edges, except at the leading edge of finite width panels where they are located 10 percent of the panel width away from the edge. THETA is the lateral outward normal direction as defined previously; it is not a meridian angle except in very simple cases. EPS is the local streamwise slope. CP is the pressure coefficient. M-LOCL is the true local Mach number. PHIX, PHIL AND PHIN are the perturbation velocity ratios to freesteam velocity in the X, lateral and normal directions. PHIL is positive in the downward or increasing panel number direction. V/VZ is the ratio of the total perturbed local velocity to freestream velocity. SS-EDGE is the source strength at the adjacent lateral edge of the panel; this is the only printed value which does not correspond to the control point location. BETA-C is the correlated β. PHIY and PHIZ are the perturbation velocity components in the Y and Z directions. Two additional numbers may be printed at the right side of the page without labels. The first one, which will include a decimal, is a total pressure ratio which arose from a blunt nose or corner solution and is attenuated as the solution marches aft. The second number is an integer and tells how many iterations were computed for the point or group of points. The maximum number of iterations allowed is five. When calculations for a row are completed, the contributions of each panel (one side only) to drag, lift and pitching moment are printed (DEL-CD, DEL-CL, DEL-CM). Then the total drag, lift and moment coefficients for both sides of the configuration and summed over all completed rows are printed as CD, CL and CM.

The results for wing with the effect of the body are in the same format as the wing-alone results described previously, and are printed after all body results are listed.

9.0 RESOURCE REQUIREMENTS

The central processor time per Mach number presently varies from 1 to 15 seconds per panel on a CDC 6600. If the input geometry is axisymmetric, the

routine only calculates one solution per streamwise location and assigns the resulting pressures to all lateral panel points, thus significantly reducing the computations required. Approximately $200{,}000_8$ words of memory are required for the analysis routine with segmentation.

ENTER COMMAND -

SUPERFLY FORWARD FUSELAGE
INITIAL DATA SET FOR PROGRAM CHECKOUT
ROTATION 60. -20. 0.
CENTER, R 180. 0. 0. 121.
CLIP -6.0-20.0 -5.0 6.0 20.0 5.0

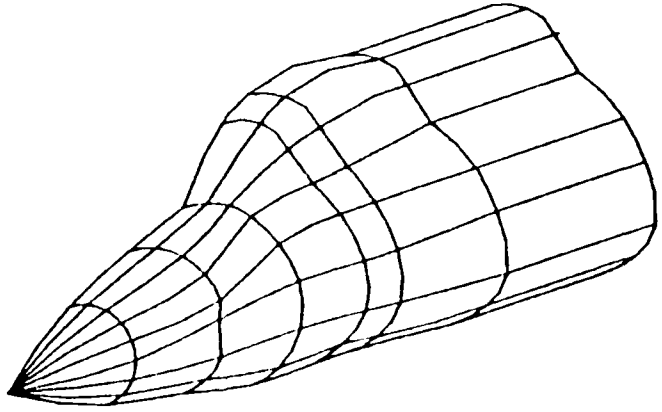

TRANSLATE
ROTATE
SCALE
CLIP
SIDES
PAINT

MARK POINTS
LOCATE POINTS

MOVE POINTS
CHANGE CORNERS
REJECT
TITLE

PRINT
PUNCH
PLOT
EXIT

FIGURE 1 SCOPE DISPLAY

```
ENTER COMMAND -
MA
ENTER POINT RANGE TO BE MARKED.
1 200
ENTER COMMAND -
LOCATE
ENTER POINT RANGE TO BE LISTED
37,45
 37  180.00     0.00   -20.00 ROU
 38  180.00     8.00   -18.00
 39  180.00    16.00   -13.00
 40  180.00    20.00    -3.00
 41  180.00    18.50     8.00
 42  180.00    15.00    16.00 CYY
 43  180.00    12.81    24.49
 44  180.00     8.50    31.50
 45  180.00     0.00    34.00
ENTER COMMAND -
MOVE
ENTER POINT RANGE AND NEW X,Y,Z
40 42 180 24 -3
```

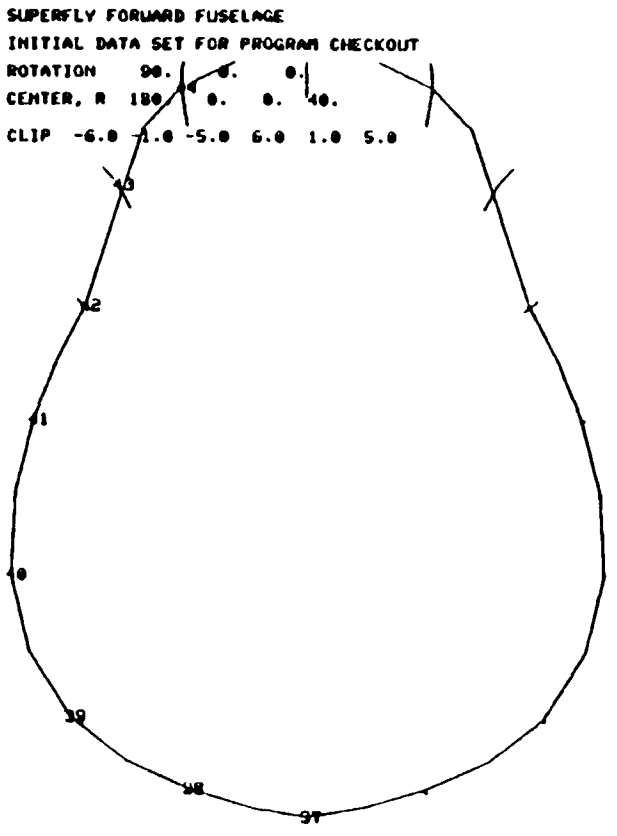

TRANSLATE

ROTATE

SCALE

CLIP

SIDES

PAINT

MARK POINTS

LOCATE POINTS

MOVE POINTS

CHANGE CORNERS

REJECT

TITLE

PRINT

PUNCH

PLOT

EXIT

FIGURE 2 STATION DISPLAY

```
12/14/82  11.34.42.
7.5 DEGREE CONE AT 12 DEG. ALPHA

 1  0.  0.  0.  S                                  0.00000    0.00000    0.00000 SEC
 2  *                                              0.00000    0.00000    0.00000
 3  *                                              0.00000    0.00000    0.00000
 4  *                                              0.00000    0.00000    0.00000
 5  *                                              0.00000    0.00000    0.00000
 6  *                                              0.00000    0.00000    0.00000
 7  *                                              0.00000    0.00000    0.00000
 8  *                                              0.00000    0.00000    0.00000
 9  *                                              0.00000    0.00000    0.00000
10  *                                              0.00000    0.00000    0.00000
11  *                                              0.00000    0.00000    0.00000

12  10000.  0.  -1316.525  R                       10000.000      0.000  -1316.525 ROW
13  *  228.4122  -1296.524                         10000.000    228.612  -1296.524
14  *  658.2625  -1140.1442                        10000.000    658.263  -1140.144
15  *  1009.5188  -846.246                        10000.000   1008.517   -846.246
16  *  1237.1298  -450.2782                       10000.000   1237.129   -450.278
17  *  1316.525  0.                               10000.000   1316.525      0.000
18  *  1237.1298  450.2782                       10000.000   1237.129    450.278
19  *  1009.5188  846.246                        10000.000   1008.517    846.246
20  *  658.2625  1140.1442                       10000.000    658.263   1140.144
21  *  228.4122  1296.524                        10000.000    228.612   1296.524
22  *  0.  1316.525                              10000.000      0.000   1316.525
```

FIGURE 3 SAMPLE CASE

SPEED .54451E+07 GAP= 10000.

IMAGES 1.6000

1 SECTIONS

SECTION	FIRST PT	FIRST ROW	ROWS	PTS/ROW
1	1	1	2	11

FIGURE 3 (CONTINUED)

FIGURE 3 (CONTINUED)

7.5 DEGREE CONE AT 12 DEG. ALPHA

/GEOMIN/ CONTENTS
NSECS= 1 = NUMBER OF SECTIONS
NROWS= 1 = NUMBER OF ROWS
NPANL= 11 = NUMBER OF PANELS, INCLUDING DUMMIES
LDISC= 0 = NUMBER OF LATERAL SLOPE DISCONTINUITIES
NKLVWG= 0 = NUMBER OF COVERED PANELS
JSTRT= 1 = ROW NUMBERS BEGINNING SECTIONS

****

ROW 1 NPL= 10

PANEL 1 ISLOISC= 0 LD= 0 ROD= -.0000

	X	Y	YD	Z	ZD	SLOPE	THETA	1/RADIUS	ARC-THETA
SIDE 1									
FWD	0.0000	0.0000	0.0000	0.0000	-.0787	-.0787	90.00	19.8902	90.01
MID	5027.5985	0.0000		-395.6806		-.0787	90.00	.0015	90.01
AFT	10055.1969	0.0000	0.0000	-791.3611	-.0787	-.0787	90.00	.0008	90.01
SIDE 2									
FWD	0.0000	0.0000	.0227	0.0000	-.0807	-.0755	80.04	19.8902	80.05
MID	5025.5193	114.3061		-405.4625		-.0755	80.04	.0015	80.05
AFT	10051.0385	228.6122	.0227	-810.9251	-.0807	-.0755	80.04	.0008	80.05

PANEL 2 ISLOISC= 0 LD= 0 ROD= -.0000

	X	Y	YD	Z	ZD	SLOPE	THETA	1/RADIUS	ARC-THETA
SIDE 1									
FWD	0.0000	0.0000	.0227	0.0000	-.0807	-.0755	80.04	19.8902	80.01
MID	5025.5193	114.3061		-405.4625		-.0755	80.04	.0015	80.01
AFT	10051.0385	228.6122	.0227	-810.9251	-.0807	-.0755	80.04	.0007	80.01
SIDE 2									
FWD	0.0000	0.0000	.0657	0.0000	-.0962	-.0509	60.26	19.8902	60.24
MID	5009.2627	329.1313		-481.9438		-.0509	60.26	.0015	60.24
AFT	10018.5253	658.2625	.0657	-963.8876	-.0962	-.0509	60.26	.0008	60.24

PANEL 3 ISLOISC= 0 LD= 0 ROD= .0000

	X	Y	YD	Z	ZD	SLOPE	THETA	1/RADIUS	ARC-THETA
SIDE 1									
FWD	0.0000	0.0000	.0657	0.0000	-.0962	-.0509	60.26	19.8902	60.22
MID	5009.2627	329.1313		-481.9438		-.0509	60.26	.0015	60.22
AFT	10018.5253	658.2625	.0657	-963.8876	-.0962	-.0509	60.26	.0007	60.22
SIDE 2									
FWD	0.0000	0.0000	.1013	0.0000	-.1257	-.0048	40.57	19.8902	40.53
MID	4978.7102	504.2583		-625.6817		-.0048	40.57	.0015	40.53
AFT	9957.4204	1008.5166	.1013	-1251.3634	-.1257	-.0048	40.57	.0007	40.53

PANEL 4 ISLOISC= 0 LD= 0 ROD= -.0000

	X	Y	YD	Z	ZD	SLOPE	THETA	1/RADIUS	ARC-THETA
SIDE 1									
FWD	0.0000	0.0000	.1013	0.0000	-.1257	-.0048	40.57	19.8902	40.54
MID	4978.7102	504.2583		-625.6817		-.0048	40.57	.0015	40.54
AFT	9957.4204	1008.5166	.1013	-1251.3634	-.1257	-.0048	40.57	.0007	40.54
SIDE 2									
FWD	0.0000	0.0000	.1253	0.0000	-.1659	.0573	21.07	19.8902	21.04
MID	4937.5471	618.5644		-819.3392		.0573	21.07	.0015	21.04
AFT	9875.0941	1237.1288	.1253	-1638.6784	-.1659	.0573	21.07	.0007	21.04

PANEL 5 ISLOISC= 0 LD= 0 ROD= .0000

	X	Y	YD	Z	ZD	SLOPE	THETA	1/RADIUS	ARC-THETA
SIDE 1									
FWD	0.0000	0.0000	.1253	0.0000	-.1659	.0573	21.07	19.8902	21.05
MID	4937.5471	618.5644		-819.3392		.0573	21.07	.0014	21.05

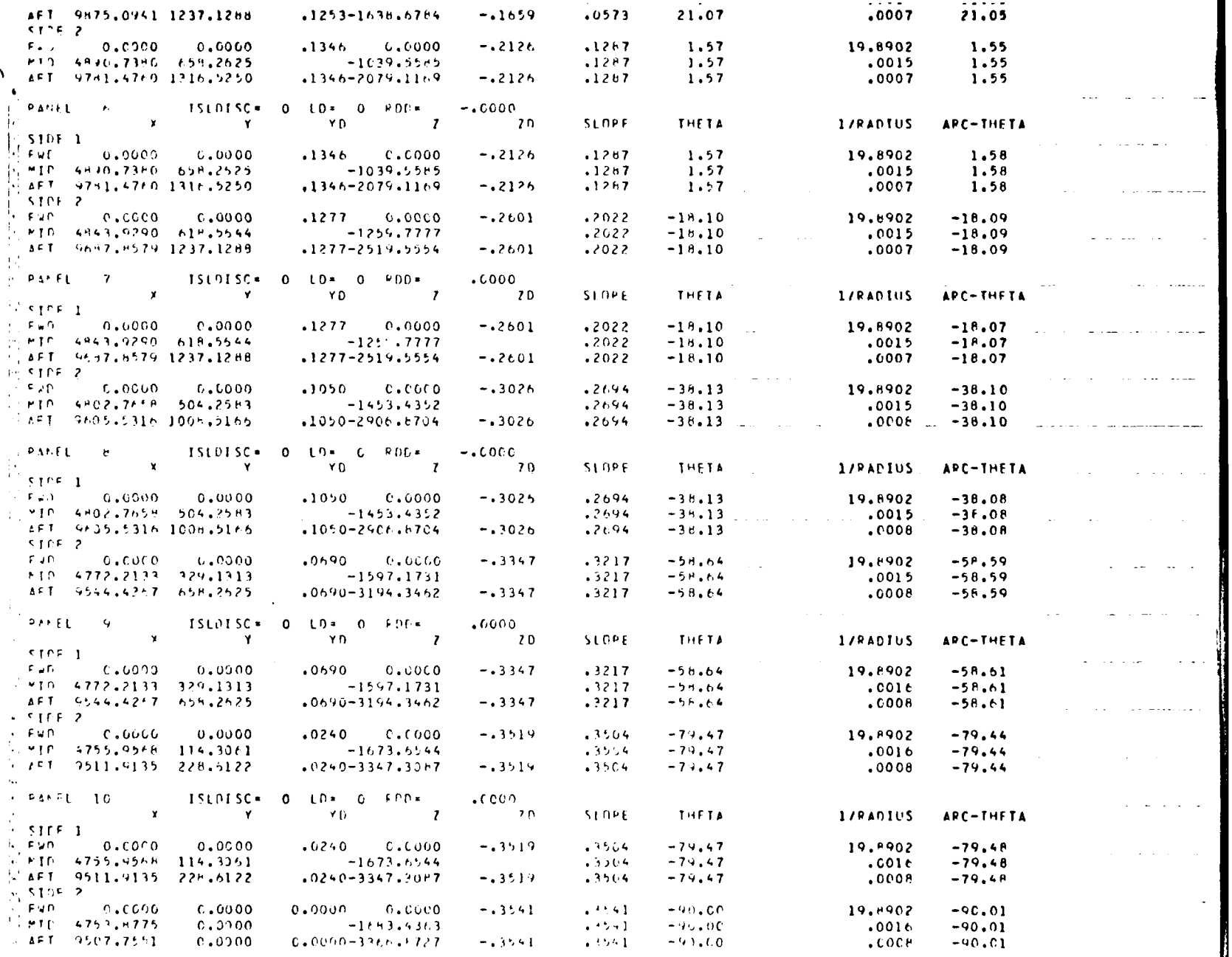

```
AFT  9875.0941 1237.1288     .1253-1638.6784   -.1659    .0573    21.07                .0007     21.05
SIDE 2
FWD     0.0000    0.0000     .1346    0.0000   -.2126    .1287    1.57              19.8902     1.55
MID  4940.7380  658.2625          -1039.5585              .1287    1.57               .0015     1.55
AFT  9741.4760 1316.5250     .1346-2079.1169   -.2126    .1287    1.57               .0007     1.55

PANEL  6        ISLDISC=  0  LD=  0  RDD=     -.0000
               X          Y          YD          Z          ZD       SLOPE     THETA          1/RADIUS   ARC-THETA
SIDE 1
FWD     0.0000    0.0000     .1346    0.0000   -.2126    .1287    1.57              19.8902     1.58
MID  4940.7380  658.2625          -1039.5585              .1287    1.57               .0015     1.58
AFT  9741.4760 1316.5250     .1346-2079.1169   -.2126    .1287    1.57               .0007     1.58
SIDE 2
FWD     0.0000    0.0000     .1277    0.0000   -.2601    .2022   -18.10              19.8902   -18.09
MID  4843.9290  618.5544          -1259.7777              .2022   -18.10               .0015   -18.09
AFT  9687.8579 1237.1288     .1277-2519.5554   -.2601    .2022   -18.10               .0007   -18.09

PANEL  7        ISLDISC=  0  LD=  0  RDD=      .0000
               X          Y          YD          Z          ZD       SLOPE     THETA          1/RADIUS   ARC-THETA
SIDE 1
FWD     0.0000    0.0000     .1277    0.0000   -.2601    .2022   -18.10              19.8902   -18.07
MID  4843.9290  618.5544          -125 .7777              .2022   -18.10               .0015   -18.07
AFT  9687.8579 1237.1288     .1277-2519.5554   -.2601    .2022   -18.10               .0007   -18.07
SIDE 2
FWD     0.0000    0.0000     .1050    0.0000   -.3026    .2694   -38.13              19.8902   -38.10
MID  4802.7658  504.2583          -1453.4352              .2694   -38.13               .0015   -38.10
AFT  9605.5316 1008.5166     .1050-2906.8704   -.3026    .2694   -38.13               .0008   -38.10

PANEL  8        ISLDISC=  0  LD=  0  RDD=     -.0000
               X          Y          YD          Z          ZD       SLOPE     THETA          1/RADIUS   ARC-THETA
SIDE 1
FWD     0.0000    0.0000     .1050    0.0000   -.3026    .2694   -38.13              19.8902   -38.08
MID  4802.7658  504.2583          -1453.4352              .2694   -38.13               .0015   -38.08
AFT  9605.5316 1008.5166     .1050-2906.8704   -.3026    .2694   -38.13               .0008   -38.08
SIDE 2
FWD     0.0000    0.0000     .0690    0.0000   -.3347    .3217   -58.64              19.8902   -58.59
MID  4772.2133  329.1313          -1597.1731              .3217   -58.64               .0015   -58.59
AFT  9544.4267  658.2625     .0690-3194.3462   -.3347    .3217   -58.64               .0008   -58.59

PANEL  9        ISLDISC=  0  LD=  0  RDD=      .0000
               X          Y          YD          Z          ZD       SLOPE     THETA          1/RADIUS   ARC-THETA
SIDE 1
FWD     0.0000    0.0000     .0690    0.0000   -.3347    .3217   -58.64              19.8902   -58.61
MID  4772.2133  329.1313          -1597.1731              .3217   -58.64               .0016   -58.61
AFT  9544.4267  658.2625     .0690-3194.3462   -.3347    .3217   -58.64               .0008   -58.61
SIDE 2
FWD     0.0000    0.0000     .0240    0.0000   -.3519    .3504   -79.47              19.8902   -79.44
MID  4755.9548  114.3061          -1673.6544              .3504   -79.47               .0016   -79.44
AFT  9511.9135  228.6122     .0240-3347.3087   -.3519    .3504   -79.47               .0008   -79.44

PANEL 10        ISLDISC=  0  LD=  0  RDD=      .0000
               X          Y          YD          Z          ZD       SLOPE     THETA          1/RADIUS   ARC-THETA
SIDE 1
FWD     0.0000    0.0000     .0240    0.0000   -.3519    .3504   -79.47              19.8902   -79.48
MID  4755.9548  114.3061          -1673.6544              .3504   -79.47               .0016   -79.48
AFT  9511.9135  228.6122     .0240-3347.3087   -.3519    .3504   -79.47               .0008   -79.48
SIDE 2
FWD     0.0000    0.0000    0.0000    0.0000   -.3541    .3541   -90.00              19.8902   -90.01
MID  4753.8775    0.0000          -1683.4383              .3541   -90.00               .0016   -90.01
AFT  9507.7551    0.0000    0.0000-3366.8727   -.3541    .3541   -90.00               .0008   -90.01
```

FIGURE 3 (CONTINUED)

FIGURE 3 (CONTINUED)

MODIFIED LINEAR THEORY WAVE DRAG ROUTINE
NON-AXISYMMETRIC BODY

MACH NUMBER = 1.6000
12/14/82 11.34.42. 7.5 DEGREE CONE AT 12 DEG. ALPHA

X	Y	Z	THETA	EPS	CP	M-LOCL	PHIX	PHIL	PHIN	V/VZ	SS-EDGE	BETA-C	PHIY	PHIZ
1.0055	.0045963	-.0792153	86.02	-.0781	.0177	1.579	-.0118	-.0052	-.0772	.9912	-.0873	1.2218	-.0079	-.0770
1.0055	.0219004	-.0930394	76.06	-.0706	.0041	1.595	-.0061	-.0556	-.0701	.9979	-.0861	1.2425	-.0708	-.0547
1.0055	.0340037	-.1016535	66.28	-.0616	-.0245	1.630	.0052	-.1127	-.0419	1.0124	-.0640	1.2888	-.1170	.0277
1.0055	.1077499	-.1337676	36.64	.0077	-.0449	1.696	.0117	-.1506	.0078	1.0229	-.0424	1.3238	-.0836	.1255
1.0055	.1291120	-.1759322	17.15	.0716	-.0501	1.663	.0112	-.1549	.0724	1.0256	.0041	1.3331	.0235	.1693
1.0055	.1352710	-.2234312	-2.35	.1434	-.0211	1.626	-.0088	-.1374	.1420	1.0107	.0548	1.2832	.1475	.1315
1.0055	.1250580	-.2766636	-22.08	.2155	.0469	1.552	-.0480	-.1041	.2051	.9799	.1020	1.1876	.2307	.0230
1.0055	.0992906	-.3117478	-42.18	.2798	.1283	1.458	-.0943	-.0792	.2520	.9367	.1296	1.0729	.2399	-.1105
1.0055	.0608451	-.3412913	-62.78	.3274	.1866	1.399	-.1350	-.0471	.2832	.9114	.1577	1.0036	.1714	-.2302
1.0055	.0193728	-.3546492	-81.58	.3511	.2334	1.357	-.1590	-.0186	.2953	.8916	.1650	.9517	.0617	-.2894
1.0055	.0045596	-.3559847	-87.90	.3534	.2381	1.353	-.1613	.0036	.2964	.8895	.1641	.9461	.0072	-.2963

PANEL NO.	DEL-CD	DEL-CL	DEL-CM
1	-.00318	-.00230	.00155
2	.00326	.00393	-.00264
3	.00340	.01116	-.00746
4	-.00052	.01025	-.00672
5	-.00132	.00329	-.00200
6	.00084	.00132	-.00099
7	.00848	.01729	-.01267
8	.01930	.03847	-.03488
9	.02841	.07917	-.05758
10	.01670	.04705	-.03357

CD= .1455 CL= .439 CM= -.3119
CP TIME = 15.567
STOP - NO DATA

END

DATE
FILMED

9 — 83

DTIC